AN ALTERNATIVE FRAGMENTATION THEORY FOR A MELT DROPLET AND VISUAL DATA ANALYSIS OF THE LARGE-SCALE STEAM EXPLOSIONS

by

Hakan Saip Papuççuoğlu

BS. in I.E., Istanbul Technical University, 1985

MS. in M.E., Istanbul Technical University, 1988

Post Grad. Diploma in A.E., von Karman Institute, 1991

Submitted to the Institute for Graduate Studies in Science and Engineering in partial fulfillment of the requirements for the degree of

Doctor

of

Philosophy

Boğazici University

2001

ACKNOWLEDGEMENTS

The author would like to gratefully acknowledge the valuable advices, continuous support and encouragement given by his supervisor Prof. Dr. Fahir Borak throughout this PhD. study. Helpful suggestions of the thesis committee members are appreciated, as well.

The author would also like to express his sincere gratitude to Dr. Moriyama who gave the author a written permission to use the large-scale steam explosion data that have been previously obtained by the researchers of the Severe Accident Research Laboratory of Japan Atomic Energy Research Institute (JAERI).

Special thanks are extended to all of the Severe Accident Research Laboratory members of JAERI including the former head, Dr. Sugimoto, for their kind helps during the period when the author stayed in JAERI and contributed to the digitalization of the above mentioned visual data. Their advices about the Japanese culture and Japan where the author lives are appreciated, as well.

The author would like to state his heartfelt thanks to his mother not only for the help he got during his Ph.D. study, but also for the precious support he received during his life.

ABSTRACT

AN ALTERNATIVE FRAGMENTATION THEORY FOR A MELT DROPLET AND VISUAL DATA ANALYSIS OF THE LARGE-SCALE STEAM EXPLOSIONS

An alternative fragmentation theory has been suggested for the steam explosion phenomenon. Under the conditions of the large-scale steam explosion experiments previously done by the members of Japan Atomic Energy Research Institute, model conservation equations have been solved and the maximum heat transfer coefficient is calculated as $h = 25.182x10^{6}\ Wm^{-2}K^{-1}$. Using this heat transfer coefficient, expansion velocity of the steam water interface has been calculated as about 1800 m/s. It was demonstrated that this interface velocity as a result of local explosive steam production is high enough to obtain a shock wave, which is necessary to have a large-scale steam explosion.

To have an overall understanding about the whole steam explosion process and the relation among its stages, above mentioned data have been examined and evaluated in detail. Using the debris size distribution regarding to this data, it has been found out that surface area enlargement of the melt fragments for an experiment resulted in explosion is about seven times greater than that for a no-explosion experiment done using the same amount of melt and water. Qualitative examination of the visual data revealed that steam production per unit time during an explosion is thousands of times greater than that in the case of no-explosion. Therefore, only area enlargement cannot explain the huge amount of heat transfer. Another approach, as suggested in the present work, which considers the relative velocities of the melt and the coolant, should be considered.

ÖZET

ERİMİŞ METAL DAMLASININ PARÇALANMASINA İLİŞKİN FARKLI BİR TEORİ VE BÜYÜK BOYUTLARDAKİ BUHAR PATLAMASI DENEYLERİNİN ANALİZİ

Buhar patlaması olayının tetikleme aşaması için alternatif bir parçalanma teorisi önerildi. Japon Atom Enerjisi Araştırma Enstitüsü'nde (JAERI) Japon araştırmacılar tarafından elde edilmiş olan büyük boyutlardaki buhar patlaması deneylerindeki şartlar kullanılarak, önerilen teoriye ait korunum denklemleri çözüldü ve maksimum ısı transfer katsayısı $h = 25.182x10^{6}\, Wm^{-2}K^{-1}$ olarak hesaplandı. Bu ısı transfer katsayısı kullanılarak, tetikleme aşamasında üretilen buharın genişleme hızının $1800m/s$ olduğu hesaplandı. Elde edilen buhar genişleme hızının, büyük boyutlardaki buhar patlaması olayının gerek şartlarından biri olan şok dalgası oluşumu için yeterli olduğu gösterildi.

Buhar patlaması olayının aşamaları ve bu aşamalar arasındaki fiziksel ilişkinin anlaşılması için yukarıda bahsedilen deneysel veriler detaylı olarak incelendi ve yorumlandı. Deneyler sonrasında elde edilen küçük metal parçacıklarının boyutlarından yararlanılarak patlama olması halindeki yüzey alanı artışının patlama olmaması halindekinden yaklaşık yedi kat daha fazla olduğu hesaplandı. Patlama sırasında birim zamandaki buhar üretiminin patlama olmaması haline göre binlerce defa daha fazla olduğu deneylerde gözlendi. Isı transferi alanındaki yaklaşık yedi katlık artışın patlama sırasında gözlenen cok yüksek miktardaki buhar üretimini açıklayamıyacağı ifade edildi. Isı transferi alanındaki artışın yanısıra, önerilen modelde olduğu gibi göreceli hızların rol oynadığı, konveksiyon yolu ile ısı geçişinin göz önünde bulundurulması gerektiği belirtildi.

TABLE OF CONTENTS

LIST OF FIGURES

LIST OF TABLES

LIST OF SYMBOLS

A_r	Surface area of a debris particle having a radius r
B	Dimensionless time
C	Drag coefficient
C_{dcm}	Drag coefficient between the melt and the coolant
C_{dmb}	Drag coefficient between the steam bubble and melt
c	Specific heat capacity
c_p	Specific heat capacity at constant pressure
D	Diameter
D_0	Initial diameter of the droplet
ΔT	Temperature difference between the heat transfer surfaces
e	Internal energy
h	Heat transfer coefficient
J	Mass flux through the shock wave
k	Thermal conductivity
M_T	Total mass of all the debris particles
M_r	Total mass of the debris particles having a radius r
m	Mass
$\dot{m}_{steam}$	Time rate of change of steam mass
m_0	Initial mass of the droplet
m_r	The mass of one debris particle having a radius r
N	von Neuman spike
n	Number of the steam jets
On	Ohnesorge number
P	Pressure
P_{st}	Steam pressure
p_α	Probability of an in vessel steam explosion
p_{fcc}	Probability of the contact 20 per cent of the fuel with water

p_f	Probability that the diameter of the fragmented particles will be less than 4 mm
p_c	Probability of a steam explosion resulting in a containment failure
R	Radius of the imaginary control volume
r_j	Radius of the steam jet
r_m	Radius of the melt droplet
r_b	Radius of the steam bubble
S_r	Total surface area of the debris particles having a radius r
S_T	Total surface area of all the debris particles
t	Time
T_c	Cold liquid temperature
T_h	Hot liquid temperature
T_{hn}	Homogeneous nucleation temperature
T_m	Melting temperature of the hot liquid
T_{mfb}	Minimum film boiling temperature
T_i	Interface temperature
τ	Shear stress between the steam jet and the melt
u	Velocity
u_b	Velocity of the steam bubble
u_j	Velocity of the steam jet
u_s	Velocity after the shock
u_1	Free stream velocity
We	Weber number
V	Volume of unit mass
V_T	Total volume of all the debris particles
v_r	The volume of one debris particle having a radius r
x_r	The number of debris particles having a radius r
X_j	Jet penetration distance

y_r	Total mass percentage of the debris particles having a radius r
ν	Kinematic viscosity
ν_d	Kinematic viscosity of the droplet
ν_f	Kinematic viscosity of the free stream flow
μ	Dynamic viscosity
ρ	Density
ρ_d	Density of the droplet
ρ_j	Density of the steam jet
σ	Surface tension
τ	Shear stress between the steam jet and the melt

1. INTRODUCTION

An explosion can be defined as a high amount of stored energy transformation from one form to another in a very short time. Initially, this stored energy is stable in one form. A comparatively small amount of energy, which can disturb the stability, is needed to initiate the transformation. Generally, kinetic energy, which can do work on the surroundings, is the final form of this energy conversion.

When a hot liquid comes into contact and mixes with a volatile cold liquid, in some circumstances, the heat transfer rate can be so rapid that an explosion occurs. Such an explosion is known as steam explosion (also called thermal or vapor explosions, energetic fuel coolant interactions, explosive boiling, physical explosions or rapid phase-transitions). Steam explosions involve an extraordinarily complex flow field, which is highly turbulent and multiphase. The length scale of this multiphase flow field ranges from microns to kilometers. The kind of volcanic eruptions, which are classified as phereatomagmatic explosions, are the examples of the largest scale steam explosions. Phereatomagmatic volcanic eruptions are caused by the interaction of magma with the underground water. Steam explosion is one of the safety hazards taken into consideration in the severe accident analysis of the nuclear reactors, since it can threaten the integrity of the reactor components applying a destructive force. Since a nuclear reactor contains approximately 100 tons of fuel at about 3000K, theoretically and potentially there is always a danger that fuel (melt) and water (coolant) interact leading to a steam explosion. In the nuclear power plant industry, the importance of steam explosion was first realized for the liquid metal fast breeder reactor.

If a failure of normal and emergency coolant flow occurs in a reactor (LOCA), fission product decay heat can cause the reactor fuel to melt. This may result in two possible steam explosion accident cases: One of them is α -mode failure or in-vessel steam explosion, which is caused by the interaction of the molten core material with the remaining coolant in the reactor vessel. The other one is ex-vessel steam explosion. If an in vessel steam explosion takes place, the high pressure can cause the upper cover of the reactor vessel to be thrown up like a missile such that it can reach the upper boundary of the reactor containment (Figure 1.1).

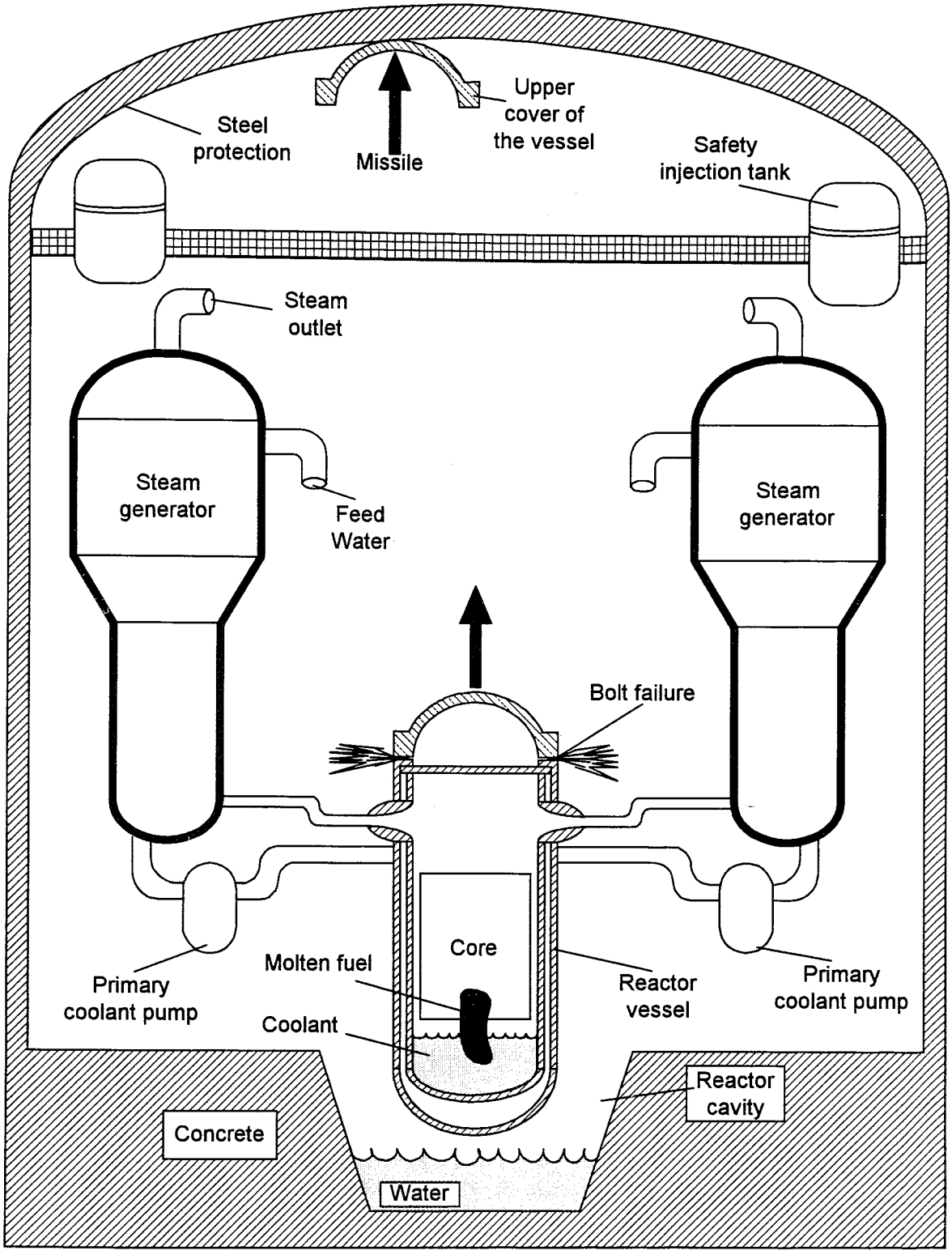

Figure 1.1. In vessel steam explosion scenario

The probability of an in vessel steam explosion in the case of a core melt down has been estimated as: $p_\alpha = p_{fcc} p_f p_c \approx 10^{-2}$ where $p_{fcc} = 1$ indicating the probability of the contact of 20 per cent of the fuel with approximately the same mass of water. $p_f = 0.1$ is the probability that the diameter of the fragmented particles will be less than 4mm. $p_c = 0.1$ is the probability that a steam explosion resulting in a containment failure occurs [1]. It is generally considered that the risk of an α-mode (in vessel) steam explosion is smaller compared to the ex-vessel case. For the ex-vessel case, the core material melts through the reactor vessel as a high temperature continuous jet and falls into the reactor cavity, which contains water to prevent the release of radioactive materials and the generation of combustible gasses [2]. The accident scenario for the ex vessel case is seen in Figure 1.2. Many scientists have performed investigations to understand the physical mechanism of steam explosion. It has been widely accepted that the fundamental mechanism of steam explosion consists of four stages: Those are coarse mixing or premixing of the two liquids, triggering, propagation (escalation) and expansion as a result of rapid heat transfer [3]. Each of those stages is very complex and not completely understood yet.

When some amount of high temperature molten metal falls into the water, the steam films cover the melt particles immediately. If the molten metal temperature is high enough, the steam film, which limits the heat transfer between the two liquids, is stable. This stage is called as coarse mixing or premixing. While the melt temperature decreases, the steam film becomes unstable, and collapses locally allowing the coolant to contact the melt. This is known as the triggering stage. Local coolant contact to the melt causes the molten metal to fragment by a physical mechanism, which is not well known yet. This fragmentation process creates a large surface area of contact allowing a large heat transfer. As a result of this large heat transfer, the coolant suddenly evaporates creating a self-propagating pressure shock wave, which causes the steam films around the other molten metals to collapse. This is usually referred to the propagation stage. Due to the direct contact of the hot liquid to the cold one, the energy is transferred very rapidly and the mixture expands very fast such that it can give damage to the surrounding structures. This is the final steam explosion stage, which is commonly known as expansion.

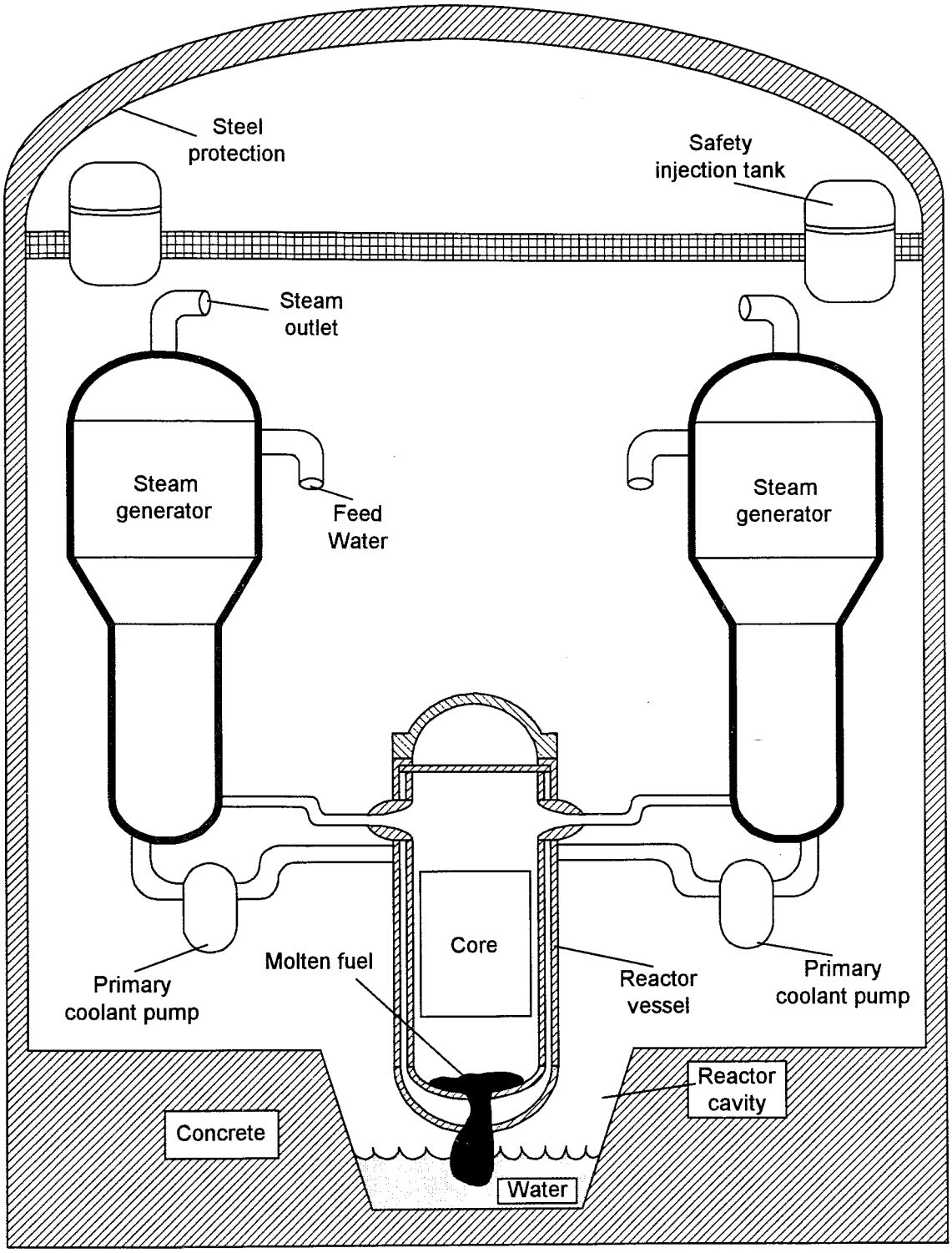

Figure 1.2. Ex vessel steam explosion scenario

Steam explosions can also be classified according to the contact geometry and relative initial velocities between the melt and the coolant in the premixing stage. If the melt falls freely into the coolant pool, the relative initial velocity between the melt and the coolant is due to the gravitational force. Because of this relative velocity, the melt is divided into smaller parts. This mode is called as pouring mode (Figure 1.3.a). In this mode, the mixing time is comparatively long. If a steam layer due to the density difference separates the coolant and the molten metal from one another, the shock wave can propagate along the surface after the triggering. This mode, which is comparatively less energetic, is called as stratified mode (Figure 1.3.b).

For the injection modes, (coolant injection and melt injection, Figure 1.3.c and d) the relative velocity between the coolant and melt is higher compared to the other modes. As a result, hydrodynamic breakup process is more effective. Therefore, finer melt particles are seen in the premixing stage [4][5]. In the real accident cases, when a big amount of molten fuel comes into contact with the coolant, a complex interaction geometry (Figure 1.3.e) involving both coolant entrapment and hydrodynamic jet breakup can take place. Since steam explosion is a very complicated multiphase, multi-component and rapid phenomenon, a complete theoretical model representing the whole process of the experimental results is not available in the literature. The details of the steam explosion process are presented schematically in Figure 1.4.

In the next chapter, after making a short literature survey, the problem has been described. The third chapter includes the explanation of a phenomenological model and the idea without mathematical expressions. In this chapter, some criticisms about the weak points of the existing literature have also been done. The fourth chapter consists of several sections. Suggestion of an analytical fragmentation theory, solution of the model conservation equations under the conditions of the large-scale steam explosion experiments, calculation of the maximum heat transfer coefficient and its evaluation i.e. whether it is high enough to create a shock wave, are the main topics discussed in the sections of the fourth chapter. Experimental apparatus (ALPHA facility of Japan Atomic Energy Research Institute) has been introduced in the fifth chapter. The evaluation of the debris size distribution and the visual data previously obtained by the JAERI members are the main topics of the sixth chapter.

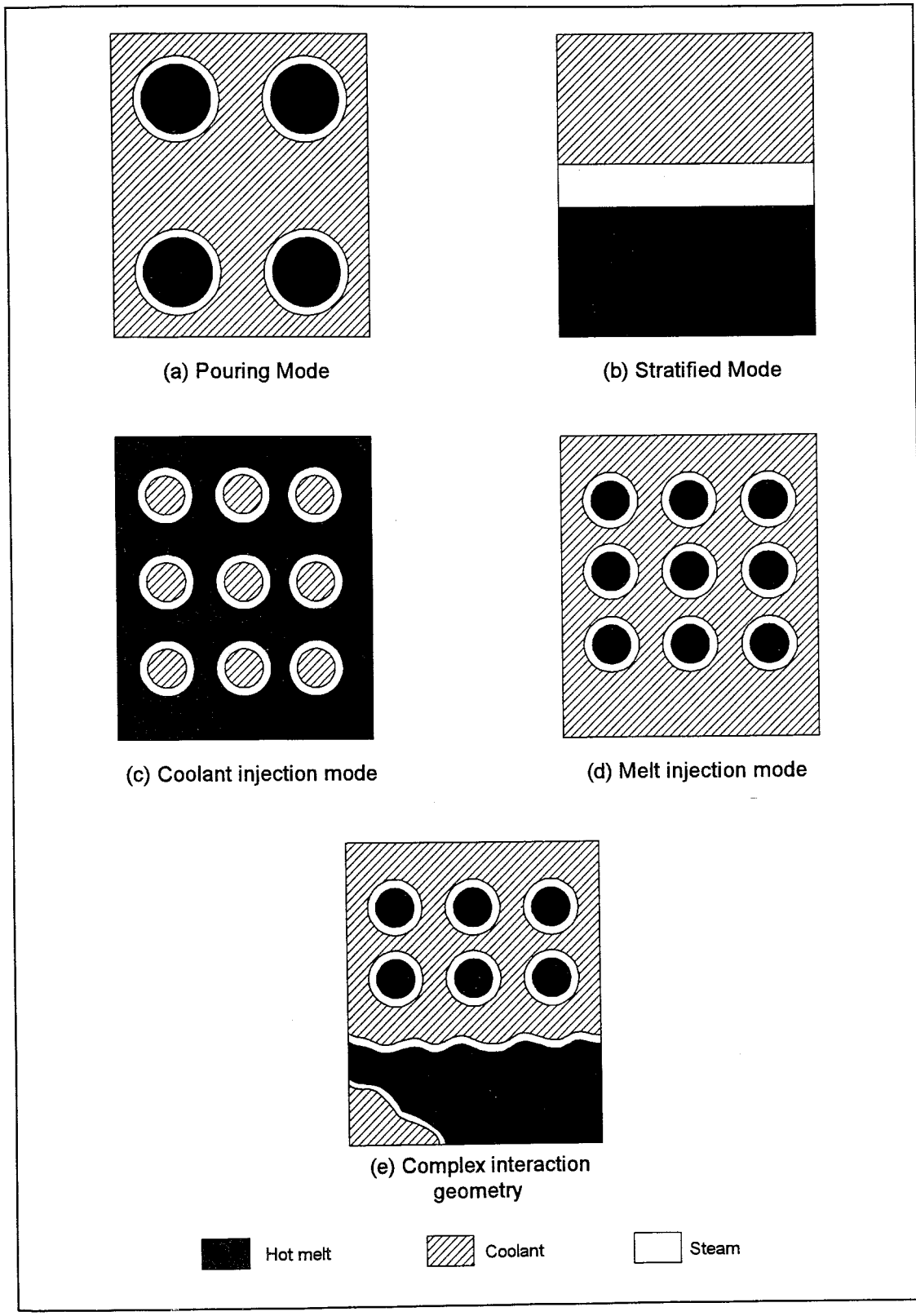

Figure 1.3. Contact geometries of the melt and coolant

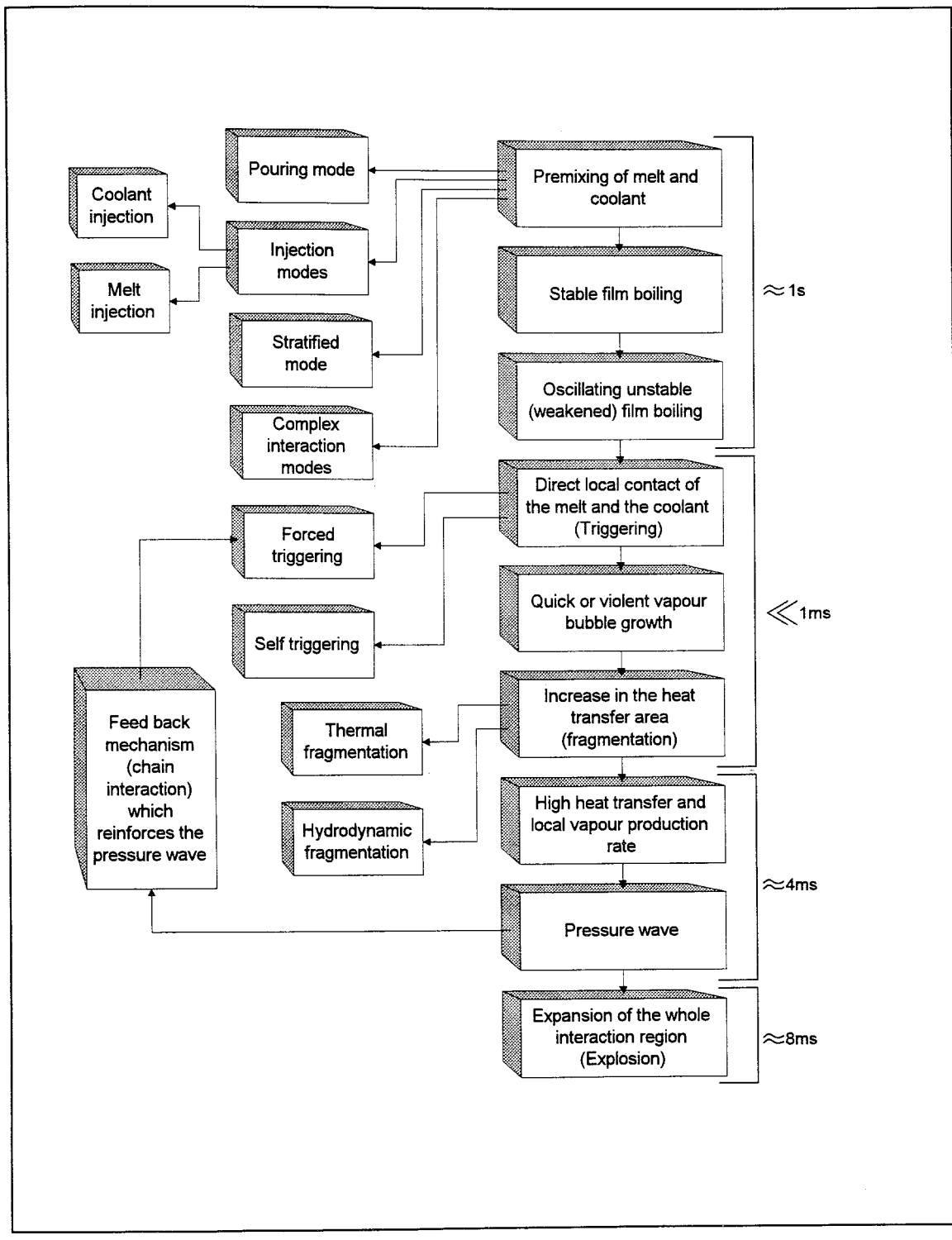

Figure 1.4. Schematic illustration of the steam explosion process

2. A BRIEF BACKGROUND AND STATEMENT OF THE PROBLEM

2.1. A Brief Background

The first investigation about steam explosion is carried out by Long [6] in 1957. In this study, it has been concluded that the liquid is trapped between the molten metal and the bottom surface of the container. The rapid liquid expansion blows the molten metal causing it to be dispersed in small particles. After that a very sudden transfer of heat forms steam fast enough to lead to a serious explosion. This theory is called as entrapment theory. To prevent steam explosion, Long suggested that the bottom of the container should be covered by grease or paint such that the small amount of liquid, which initiates the minor explosion, cannot be trapped underneath the molten.

Several researchers have suggested many theories about the different stages of steam explosion. The premixing, which is the first stage in a sequence of events leading to the explosive release of heat energy, is relatively slow (about 1 second). In principle, it is considered that the amount of melt taking part in the steam explosion and the resultant peak pressure of the explosion are strongly related to the initial mixing conditions [7]. The interaction zone of this stage has a characteristic dimension of the order of 10 mm [8]. In other words, even for the large quantities of melt, the melt mixes with the coolant such that the molten particle dimensions would be about 10mm just before the fine fragmentation step. For this stage, the important parameters are the extent of the void fraction and the degree of melt breakup. At high void fractions the explosion even cannot be triggered [9]. Although a large amount of melt is dropped inside the coolant pool, it may not result in an intensive explosion, unless a considerable amount of melt is broken-up effectively and contribute to the rapid heat transfer process [10].

Triggering is considered to be a very fast (the time scales are less than milliseconds) and localized process, which may not be noticeable at the whole scale of the incident. In steam explosion phenomenon, there are two types of triggering mechanisms: "self triggering" and "forced triggering". In forced triggering, the steam film around the hot melt collapses due to an external pressure pulse. In the self-triggering case, the steam film collapses naturally when

the interface contact temperature between the molten metal and the coolant falls below the minimum film boiling temperature [11,12].

Board and Hall assume that a disturbance shock wave propagates through a molten metal and coolant mixture causing fine fragmentation of the molten metal and rapid heat transfer from the hot metal to the coolant. This heat transfer causes the coolant to expand sustaining the propagation of the shock wave [13][14]. The pressure, velocity, density and internal energy are presented by P_1, u_1, ρ_1 and e_1, respectively, in front of the shock wave. Similarly, P_2, u_2, ρ_2, and e_2 show the same physical properties behind the shock wave. Conservation of mass, momentum and energy equations can be written across the reaction wave as:

$$u_1\rho_1 = u_2\rho_2 \equiv J \tag{2.1}$$

$$P_1 + \rho_1 u_1^2 = P_2 + \rho_2 u_2^2 \tag{2.2}$$

$$e_1 + \frac{P_1}{\rho_1} + \frac{1}{2}u_1^2 = e_2 + \frac{P_2}{\rho_2} + \frac{1}{2}u_2^2 \tag{2.3}$$

Using those equations:

$$\frac{1}{2}(P_1 + P_2)(V_1 + V_2) = e_2 + e_1 \tag{2.4}$$

Equation (2.4) is obtained. If Equation (2.4) is plotted on a P-V diagram, the dotted curve, which represents all the possible end states adiabaticaly, is obtained (Figure 2.1). Taking into consideration the sudden changes in mass and momentum across the shock wave, Equation (2.5) is obtained.

$$J = \sqrt{\frac{P_2 - P_1}{V_1 - V_2}} \tag{2.5}$$

J represents the mass flux through the shock wave. As is seen from Equation (2.5), region A-B is physically meaningless. It is also clear that the end states should also be on a straight line passing from point "O" and having a slope $-J^2$. The intersection point of

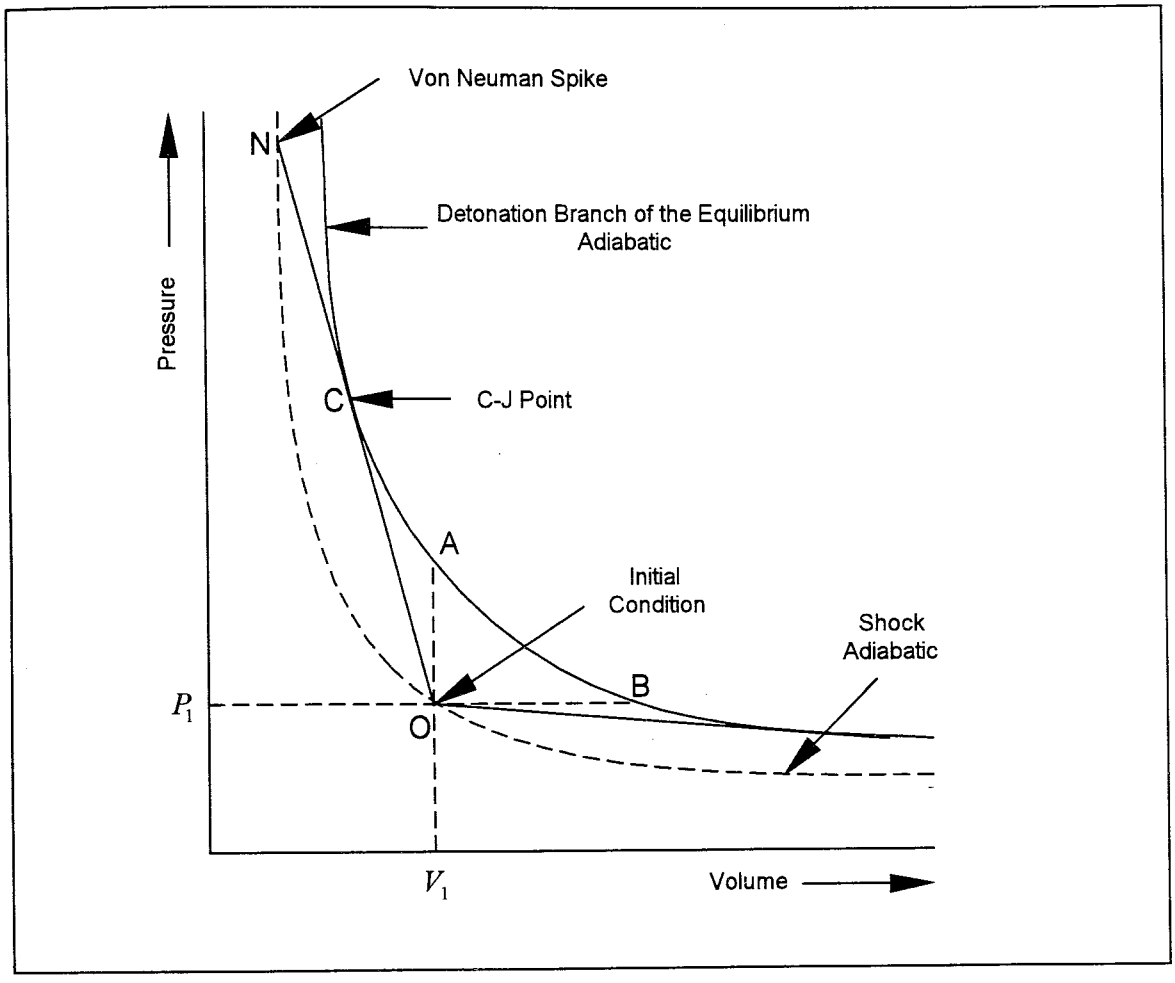

Figure 2.1. The detonation trajectory in P-V diagram [15]

this line and detonation adiabatic is called as Chapman-Jouguet (C-J) point indicating the minimum mass flux and propagation velocity, which is always supersonic. At first, the mixture is compressed up to the point N -highest pressure value known as Von Neuman spike- when it enters the shock wave. Then while the reaction takes place through the shock, the pressure decreases until the pressure level at the point C [14].

Although Board-Hall model is one of the milestones of the investigation of the large-scale steam explosion phenomenon, a couple of years later, it has been understood that there are some important physical differences between the conceptual explanation of Board-Hall

model and the experimentally observed real situations. For example, Board-Hall model assumes that the medium before the shock arrives is homogeneous. However, this is not the case that can usually be met in the real accidents or experiments. In the real situations, the escalation from a trigger to a steady state detonation is very complex and not completely understood yet. Whereas, Board-Hall model assumes that the shock wave has a constant speed. It is also assumed that all of the molten metal interacts with all of the coolant. This is also incorrect for most of the real accident cases. The model does not take into consideration the details of the fragmentation, mixing and heat transfer process. The model accepts that all those complex phenomena occur inside the reaction zone moving with the shock wave where the thermal and mechanical equilibrium is reached [15,16]. The critical conditions required to support a self-sustained propagating interaction are not known, because of the difficulties in determining the pressure, temperature, velocity fields and the initial premixing conditions.

Another theory to explain the fragmentation process is suggested by Groenveld [17]. According to this theory, the stagnation pressure at the front of the moving hot drop will cause the melt drop to decelerate. This deceleration of the front part of the melt droplet leads to a deformation such that the melt drop changes its shape from spherical to a flat shape like a disk. Then, under the effect of interfacial tension, the sides move inward and forward while the center moves backward. The combination of those motions causes a small amount of coolant to be trapped inside the hot liquid. After that, the trapped coolant can shatter the melt on evaporation. This is called as encapsuling theory.

If the molten particle exceeds either the critical size or the critical velocity, the inertial forces exerted on the melt by the coolant can overcome the surface tension of the melt. This causes the molten mass to split into many parts. The critical conditions are determined by the Weber Number, which is the ratio of the destabilizing inertial force to the stabilizing force due to the surface tension.

$$We = \frac{\rho . u^2 r}{\sigma} \geq 10 \qquad (2.6)$$

Where ρ is the density of the coolant, u is the relative velocity between the molten metal and the coolant, r is the radius of the melt droplet and σ is the interfacial tension.

The temperatures of the coolant and the molten metal play an important role in steam explosions. In Figure 2.2., the shaded area indicates the thermal interaction zone (TIZ) including the coolant and the molten metal temperatures. To experience a spontaneous steam explosion both T_h (hot liquid temperature) and T_c (cold liquid temperature) should be inside the TIZ. However, some experimental studies indicated that even if the temperature conditions are within the TIZ, there cannot be any steam explosion. T_i and T_{hn} show the interface temperature of the two liquids and homogeneous nucleation temperature of the cold liquid, respectively. As is seen from Figure 2.2., T_i should at least be equal to T_{hn} in order to have an explosion. On the contrary, upper limits of T_i and T_{hn} depend on the experimental conditions. In the case that the melting temperature of the hot liquid T_m is smaller than T_{hn} the steam explosion may occur, since the hot material is in liquid state and it can fragment easily. Whereas, when T_m is greater than T_{hn} steam explosion cannot occur, because the hot liquid becomes solid when it contacts the cold one; then it cannot fragment [18]. However, it should be pointed out that the above criterion is only a necessary condition and not a sufficient one. In order to have a steam explosion, rapid bubble growth must also occur to sustain a strong shock [19]. The interface temperature T_i is given by the following equation.

$$T_i = \frac{T_h (k\rho c_p)_h^{1/2} + T_c (k\rho c_p)_c^{1/2}}{(k\rho c_p)_h^{1/2} + (k\rho c_p)_c^{1/2}} \tag{2.7}$$

Where ρ is the density c_p is the heat capacity at constant pressure, k is the thermal conductivity and the subscripts h and c indicate hot and cold liquid, respectively [15]. In Figure 2.2., T_{hn}, the left hand border of TIZ, which is considered as the necessary condition for the steam explosion, is 302 $^{\circ}C$ for water. The inclined line (the right hand border of TIZ) can be determined by an empirical correlation indicating the minimum film boiling temperature (T_{mfb}) for water [20].

$$T_{mfb} = 201 + 8(T_{sat} - T_c) \quad (^{\circ}C) \tag{8}$$

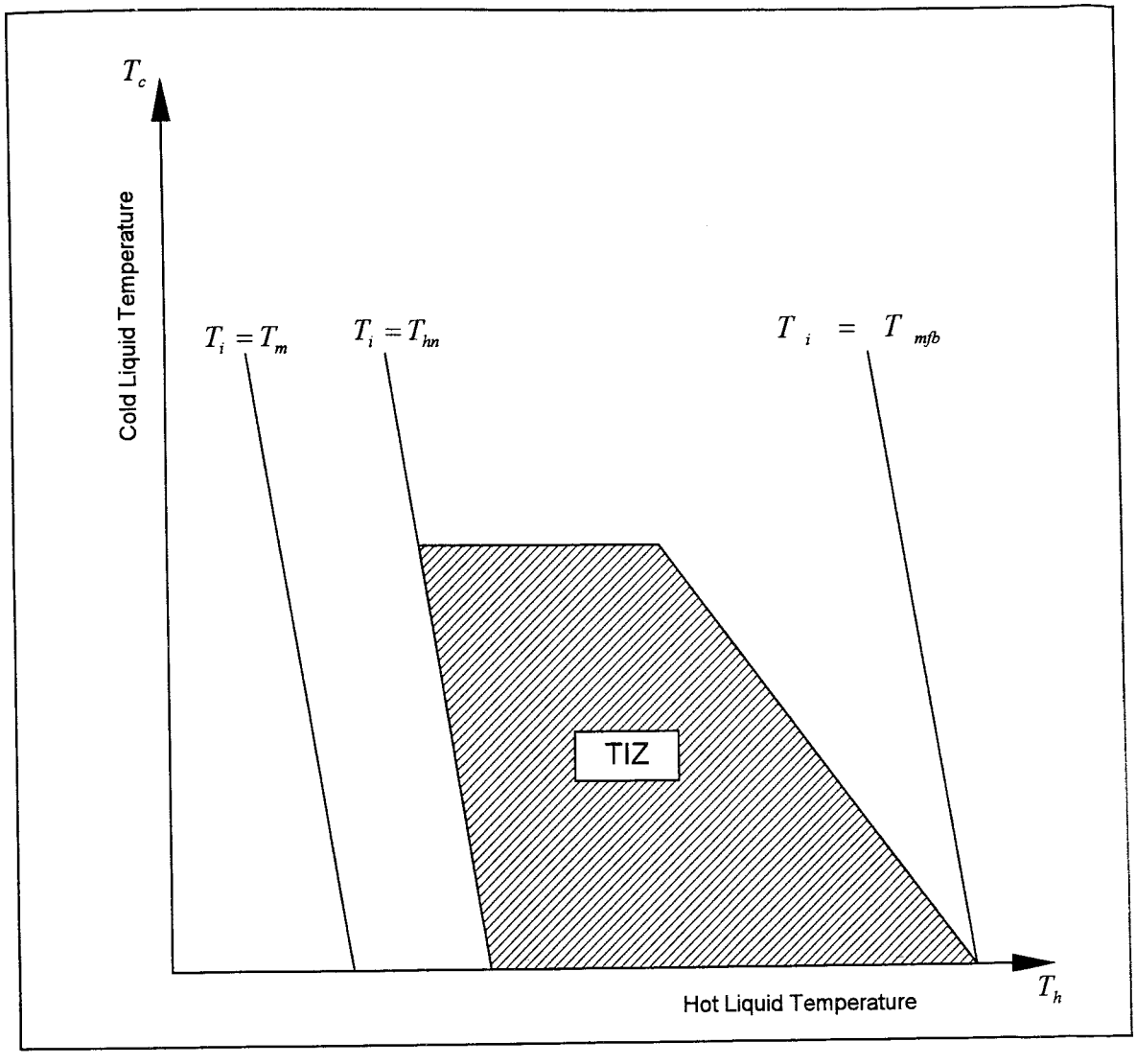

Figure 2.2. Thermal interaction zone [18]

According to the violent boiling theory, the fluid forces generated during the transition from film to nucleate boiling of the liquid may overcome the surface tension of the melt and cause it to be fragmented [17].

Another theory introduced by Epstein [21] suggests that the fragmentation of a molten metal droplet in a coolant is caused by the violent release of the dissolved gases within the molten metal. In other words, the dissolved atmospheric gases in a molten metal droplet on rapid quenching can apply high pressure causing the melt to be fragmented.

2.2. Statement of the Problem

Today, the experimental techniques and equipments are not capable enough to observe and completely understand the complicated triggering stage of the steam explosion phenomenon. In the literature, there is no complete fragmentation model representing the whole process in the microscopic level. All of the fragmentation theories (thermal and hydrodynamic) have some weak points. One of the purposes of this PhD study is to analyze the weak points of the existing theories and to suggest an alternative fragmentation model.

Steam explosion is a phenomenon consisting of several subsequent stages, which are strongly related to one another. If a melt particle is triggered, it does not mean that the triggering will result in a large-scale explosion. A continuous propagation wave reinforced by the triggering of the other melt droplets is necessary to have a steam explosion. Of course, one of the most important steam explosion stages is the premixing stage at which the necessary initial conditions are provided for the following stages such as escalation (propagation) and expansion. Unfortunately, single drop experiments give the researcher little idea about a real large-scale steam explosion. Therefore, a detailed investigation of the large-scale steam explosion experiments is important to have an overall understanding of the whole steam explosion process and the relation among its stages. This constitutes another purpose of this PhD. study. Heat transfer area enlargement as a result of fine fragmentation should be determined and evaluated to understand its contribution to the huge energy transfer in a very short time. Therefore, it is important to compare the debris size distribution of a large-scale steam explosion experiment with that of a non-explosion one. The comparison should be made on the basis of surface area enlargement.

One of the most important issues is to determine the heat transfer coefficient for the triggering stage. There are significant uncertainties concerning the heat transfer coefficient due to the extraordinarily complex flow field, which is highly turbulent, multiphase and multi-component. Available heat transfer coefficient data are rough and time averaged. One of the main targets of this PhD study is to obtain the maximum value of the heat transfer coefficient for the triggering stage under the conditions of the large-scale steam explosion experiments. And finally, it is crucial to check the validity of the calculated heat transfer coefficient. In other words, it should be demonstrated that whether the sudden steam production can result in a shock wave or not.

3. SUGGESTION OF A PHENOMENOLOGICAL MODEL

Despite the increase in surface area as a result of fine fragmentation, the necessary heat transfer per unit time for the explosive amount of steam production is much greater than that observed in the steady nucleate boiling processes [22]. None of the fragmentation models present in the literature can explain this fact properly. Fragmentation models, generally, can be classified as thermal and hydrodynamic fragmentation. Most of the thermal fragmentation models include a coolant jet penetration into the melt droplet. Subsequently, the evaporation of the trapped coolant blows off the melt [23]. When the steam film is destabilized, it starts to oscillate. If something is oscillating, it should first slowdown and then stop before the reverse motion takes place. Therefore, the oscillating coolant steam interface should first slowdown and then stop at the point where it is closest to the melt before the reverse motion takes place (Figure 3.1.). After several oscillations, the closest distance between the steam liquid interface and the melt decreases and finally, the interface boundary (liquid) contacts with the melt. However, because of the nature of the oscillation, it is expected that the coolant should slowdown before it touches the melt. Since the liquid velocity is expected to be around zero at the instant when the liquid contacts with the melt, the author thinks that the liquid does not have sufficient kinetic energy to penetrate into the melt. Let's assume that the coolant penetrates into the melt. In this case, it will take a certain period of time for the coolant to penetrate from the surface of the melt to the point inside the melt until the region where the coolant penetrates. However, the coolant finger will evaporate immediately upon contact with the melt, if the melt temperature is above the spontaneous nucleation temperature, which is a necessary condition for a steam explosion. Therefore, the author thinks that liquid coolant penetration into the melt is unlikely. In the following chapter, the author will suggest and model that some amount of steam can penetrate into the melt as a result of rapid local steam production at the contact region.

Kim and Corradini [24] suggested that needle-like coolant jets penetrate into the fuel after the steam film collapses. Subsequent expansion of those coolant jets that are entrained in the fuel near the surface, results in the fragmentation of the outer surface layer of the fuel. The same cyclic process that begins with the film collapse continues until all of the melt is

fragmented (Figure 3.2.). However, it is known that the average time period for a stable steam collapse is about one second. Therefore, this cyclic process should at least take a couple

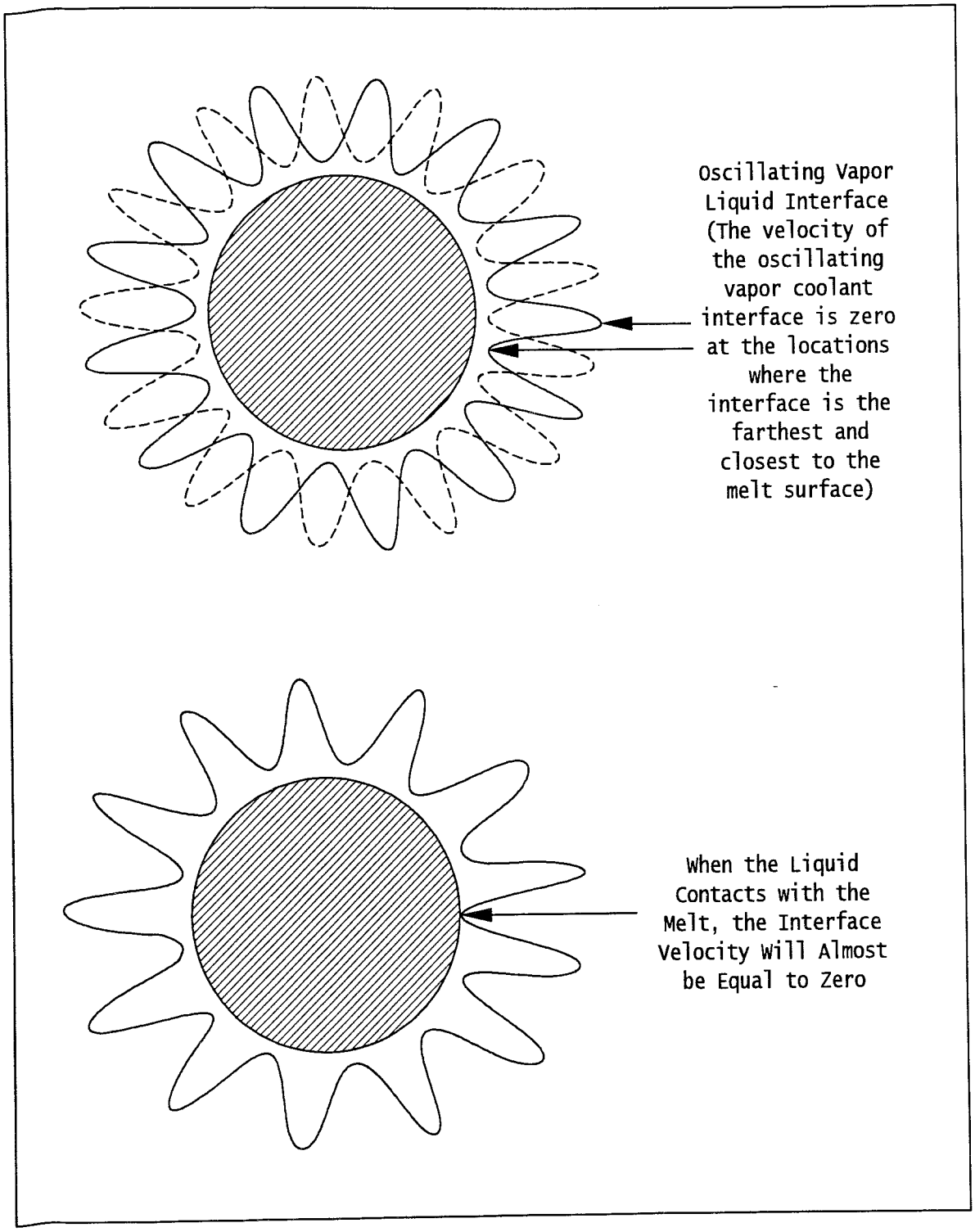

Figure 3.1. A schematic illustration of the destabilized oscillating steam film

of seconds. On the contrary, it is experimentally evident that fragmentation of a single droplet takes at most one millisecond. Therefore, the author thinks that the conflict between the experimental outputs and the theory concerning the time scale of the fragmentation process is another weak point of the above mentioned thermal fragmentation theory.

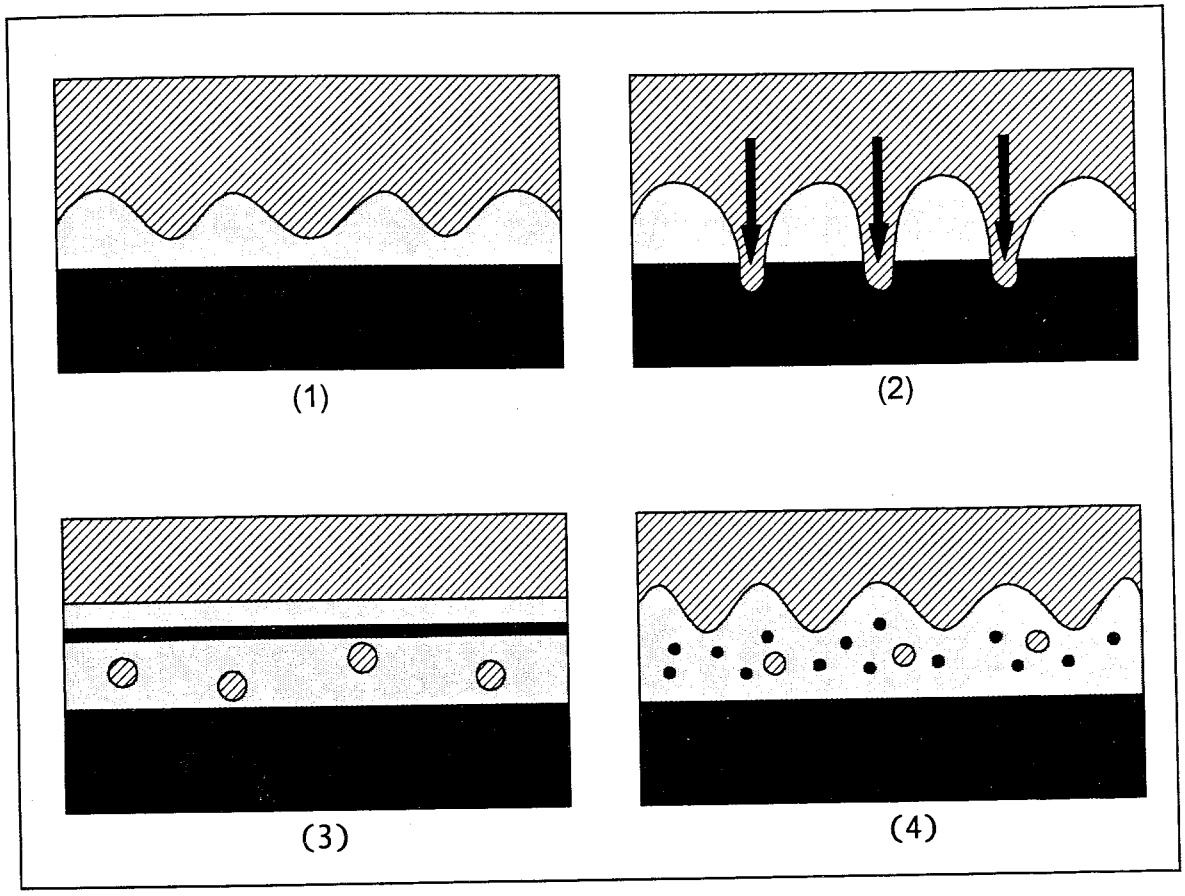

Figure 3.2. Steam explosion model proposed by Kim and Corradini

At the triggering stage, as a result of local film collapse, the hot melt comes into direct contact with the coolant. When this happens, a very high local heat transfer leads to a sudden evaporation. The author suggests that this local explosive evaporation acts as a propulsive force according to the conservation of momentum principle. Therefore, it is obvious that the triggered molten metal particle will be accelerated due to this propulsive force (Figure 3.3.). It is well known that if a liquid drop is accelerated in another fluid, the liquid droplet is fragmented [25-28]. The fragmentation takes place on the surface of the melt by means of boundary layer stripping both in the coolant and in the melt. The broken melt particles on the surface are stripped away. Since the temperature of the inner regions of the melt is higher compared to the regions closer to the surface, continuous melt breakup on the surface causes

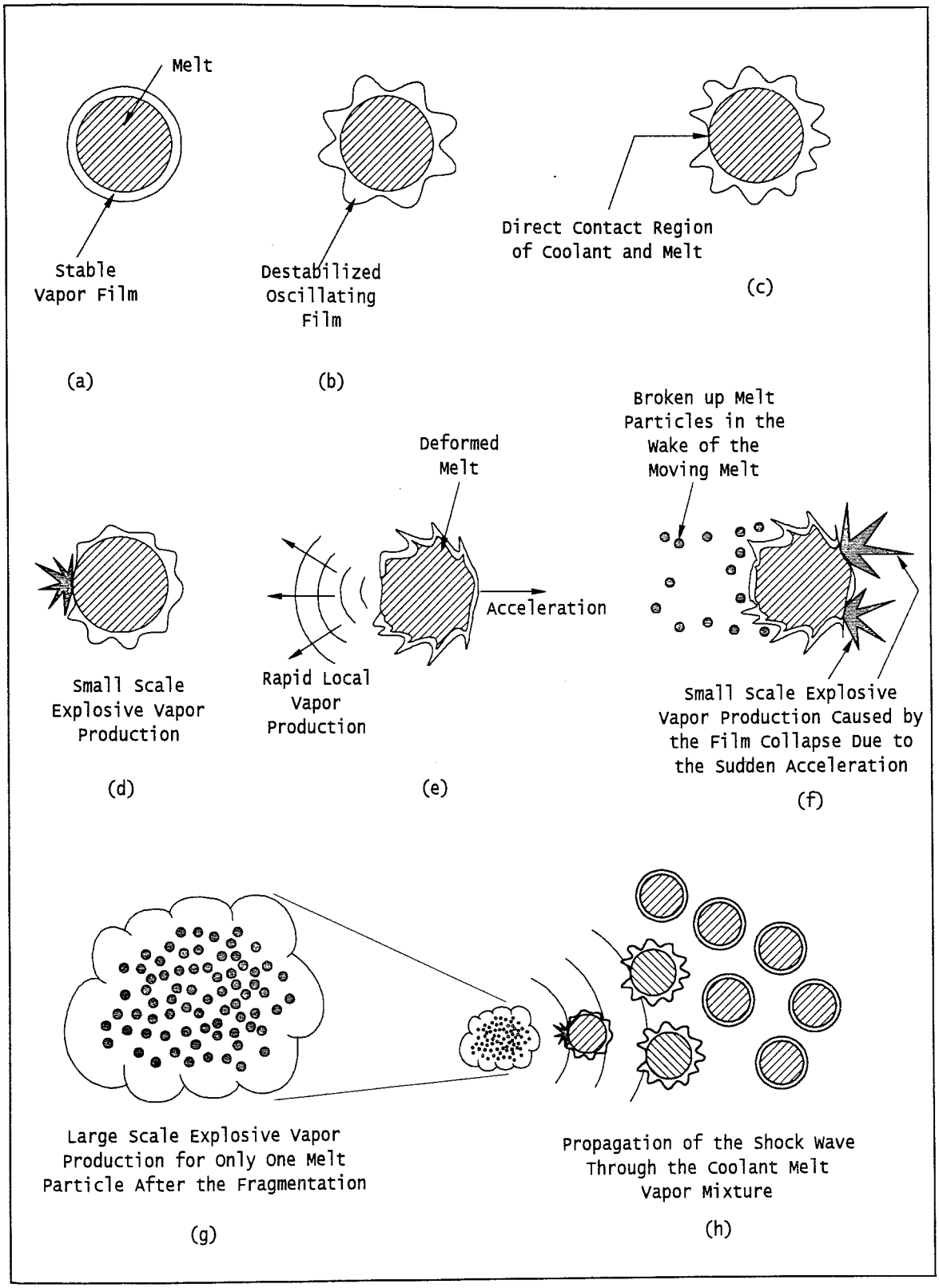

Figure 3.3. Conceptual sketch of the phenomenological model

the coolant to be exposed to the hotter regions of the melt, which is initially located inside parts of the melt. Of course, greater temperature difference between the two liquids –coolant and melt- leads to a higher heat transfer rate during the fragmentation process. The relative speed between the two liquids will also increase the heat transfer. The acceleration caused by the small-scale explosive evaporation on the contact area cannot be enough to fragment all the melt. However, the disturbance created by the acceleration can cause the destabilized steam film to collapse in some other regions on the surface. The same process (between the stages "e" and "f" in Figure 3.3.) is repeated in several different directions randomly until the whole melt is broken into its fragments. In brief, a chain reaction is initiated by the collapse of the steam film only at one small region. When the steam film is destabilized, it becomes vulnerable to the disturbances such that if it is exposed to any small disturbance, it easily collapses. Therefore, the time between the two subsequent film collapses and sudden accelerations is very short. Depending on the time, the distance between those two subsequent locations is short as well. As a result, the motion of the melt looks like a vibration in several different directions. Since the hot metal droplet is in the liquid form, it is expected that the droplet will be deformed not only by the surrounding fluid force but also by the pressure of the explosive steam production. At the triggering region a couple of steam fingers (steam jets) should penetrate into the melt. The detailed analytical explanation of this new theory will be given in the second part of the next chapter.

Hydrodynamic fragmentation mechanism has been investigated in aerodynamics. In the literature, some theoretical and empirical equations giving the stripping rate have been suggested. For example, Ranger and Nicholls [27] suggested that when a liquid drop is exposed to sudden high-speed fluid flow, the shearing action causes boundary layers to be formed both in the external flow and just under the drop surface such that the velocity of the external flow and internal flow are equal to one another on the surface of the drop (Figure 3.4.). In their investigation they suggested that the equation giving the mass breakup rate:

$$\frac{dm}{dt} = \left(\frac{3}{2}\pi^3\right)\left(\frac{\rho_f}{\rho_d}\right)^{1/3}\left(\frac{v_f}{v_d}\right)^{1/6}\left(\rho_d v_d^{1/2} u_s^{1/2} D^{3/2}\right)\left(1-\frac{u_f}{u_s}\right)^{1/2} \qquad (3.1)$$

Where ρ, v, u and D are the density, kinematic viscosity, velocity and the diameter of the drop, respectively. The subscripts f, d, and s indicate free stream, drop and the

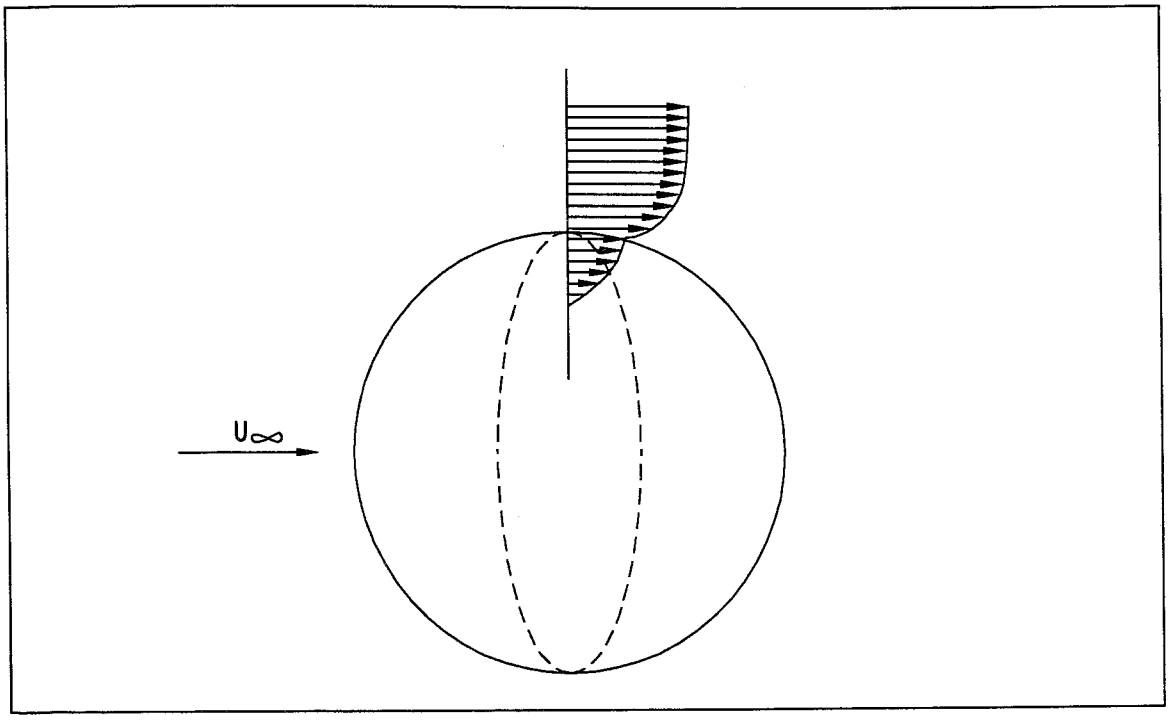

Figure 3.4. Boundary layer formation inside and outside of a droplet

conditions behind the shock, respectively. Their experimental data indicated that boundary layer stripping and breakup phenomenon occur along the equator of the droplet (dashed line in Figure 3.4.) [27].

Using x ray-radiography method, Ciccarelli and Frost [29] observed the fragmentation of a 0.5gr. drop of a low melting point alloy (49^0C) consisting of 45% bismuth, 23% lead, 19% indium, 8% tin and 5% cadmium. As a result of $4\,m/s$ average velocity water flow generated by the exploding wire, the mass is stripped away continuously from the melt surface. According to their observation, at first, the mass broken-up from the surface of the melt is in the form of long distorted filaments extending to the down stream. Later, those filaments are broken into its fine particles [29].

Waldman and Reinecke [28] have introduced another empirical formula giving the variation of droplet mass depending on time:

$$\frac{m}{m_0} = \frac{1}{2}\left(1 + \cos\left(\pi B / B_b\right)\right) \tag{3.2}$$

Where m_0 is the initial mass of the drop and the subscript b indicates breakup. B is the dimensionless time defined as:

$$B = \frac{t.u}{D_0}\left(\frac{\rho_f}{\rho_d}\right)^{1/2} \tag{3.3}$$

t and D_0 are the time and the initial diameter of the droplet, respectively. Their experimental data showed that the time for complete fragmentation due to the boundary layer stripping has a constant value ($B_b = 3.5$). A weak point of Equation (3.2) is it does not take into consideration the relative velocity decrement between the droplet and the free stream flow with time [15].

Several studies have reported that extremely viscous coolants suppress both spontaneous and triggered steam explosions [30]. The author considers that since the relative velocity of the molten metal will decrease while the viscosity of the coolant increases, the convection heat transfer rate, which is a function of relative velocity, will also decrease. Another reason of suppression of the steam explosion is the concentration of more air inside the steam film when the viscosity is increased [15]. In the first part of the next chapter, an alternative model instead of boundary layer stripping will be introduced, as well.

4. A BREAK-UP THEORY FOR A MOVING MELT

4.1. Hydrodynamic Pressure Distribution Causing the Melt to be Broken Up

As is suggested qualitatively in the previous chapter, the author believes that melt break up is mainly caused by the sudden acceleration of the melt droplet inside the surrounding liquid (coolant). If so, the hydrodynamic forces acting on the moving melt by the surrounding liquid should cause the melt to be deformed and broken up. In this chapter, the pressure applied by the coolant, and, as a result, the deformation of the melt leading to a break up process will be examined.

To set up a mathematical model, some assumptions are made. The melt droplet inside the coolant is considered as a sphere. When the relative motion of the melt is started, the flow outside the boundary layer is assumed as inviscid and subsonic. Except the region where the flow separation and a wake are formed in the downstream, the pressure at a point on the streamline just outside the thin boundary layer will be equal to the pressure on the melt. In other words, the pressure just outside the boundary layer is transmitted through it.

Let's assume that the spherical melt droplet is located in an imaginary cylindrical control volume. The radius of the imaginary cylindrical control volume and the melt droplet are R and r_m, respectively. The value of R should be equal to the distance from the center of the melt droplet to the nearest undisturbed streamline. The positions of the streamlines are seen in Figure 4.1. when the relative motion of the melt starts as a result of the triggering. From the conservation of mass inside the imaginary control volume:

$$R^2.\pi.u_1 = (R^2 - r_m^2(1 - Sin^2\varphi.Sin^2\theta))\pi.u \tag{4.1}$$

For the derivation of Equation (4.1) please see Figure 4.1. and 4.2. u_1 is the free stream velocity. u indicates the velocity along the curvature part of the streamline just outside the boundary layer depending on the position (φ and θ). If Bernoulli equation is written along a streamline just outside the boundary layer on the melt:

$$P = P_1 + \frac{\rho_{coolant}.u_1^2}{2}\left(1-\left(\frac{R^2}{R^2 - r_m^2 + r_m^2.Sin^2\varphi.Sin^2\theta}\right)^2\right) \qquad (4.2)$$

Except the region where the flow separation takes place, P shows the pressure distribution on the melt depending on φ and θ. In Equation (4.2) hydrostatic pressure difference is neglected. It is easily seen from Equation (4.2) that the pressure is the lowest when $\theta = 0$ and $\theta = \pi$. Those θ values correspond to y=0, the equator of the spherical melt in the cross flow direction. If it is assumed that the spherical melt is divided into thin circular slices perpendicular to the y axis (Figure 4.1.), the uniform pressure distribution on the lateral

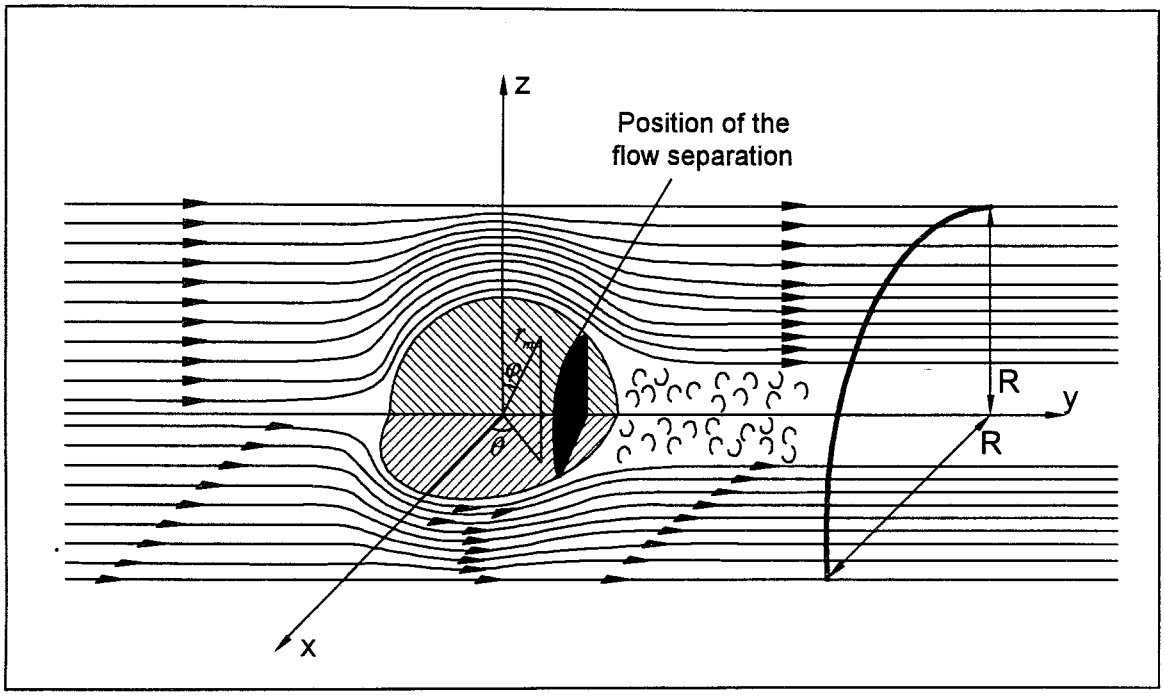

Figure 4.1. Streamlines around the moving melt

surface of the slice having a radius r_m will be the lowest. Therefore, the pressure distribution on the melt will force the melt to deform at its equator perpendicular to the y axis (lower part of Figure 4.3.). At the foot of the deformed melt total pressure –dynamic pressure + static pressure- is comparatively high depending on the velocity of the melt droplet.

The author thinks that if the total pressure depended forces at the foot of the deformed melt

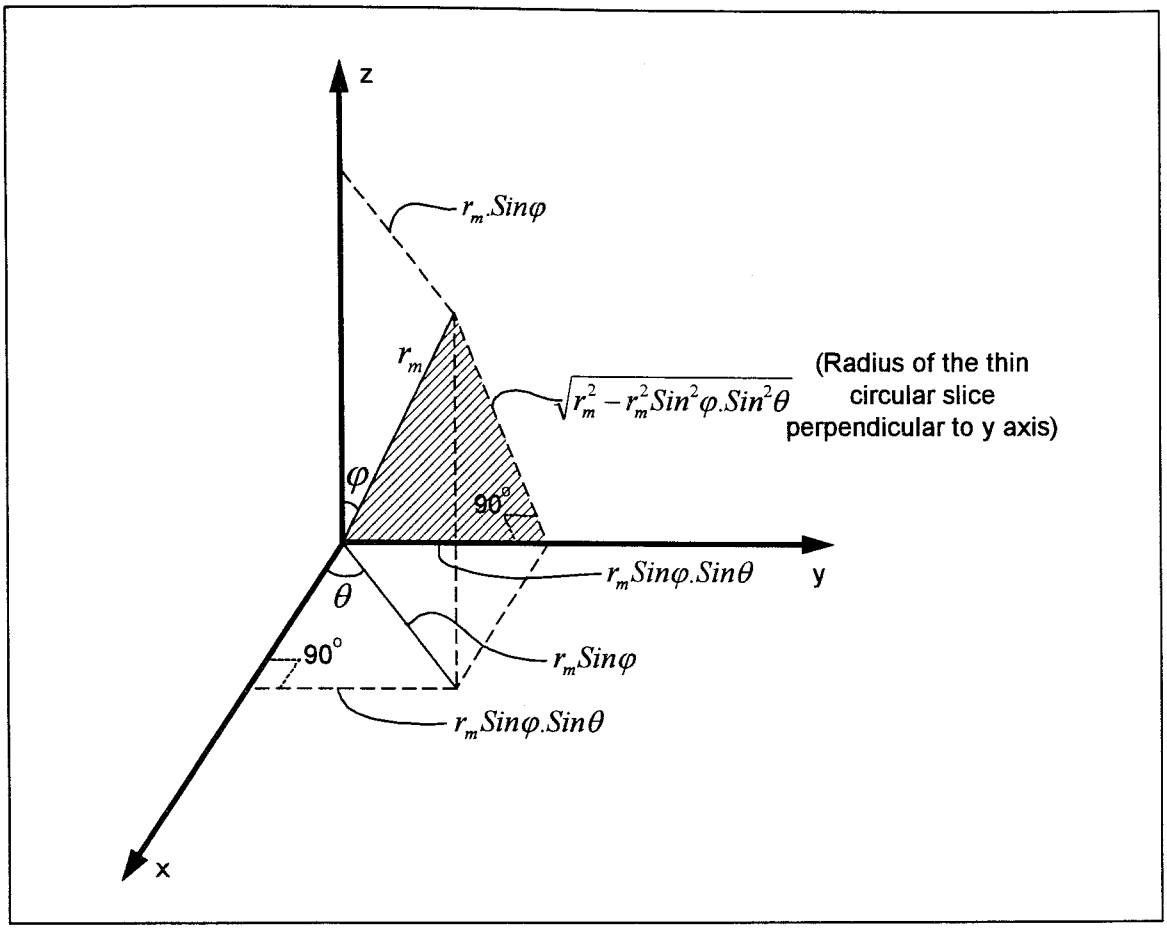

Figure 4.2. Polar coordinate system

exceeds the surface tension forces, the deformed part of the melt can be broken up (Figure 4.3.). In the literature concerning aerodynamics there are some experimental evidences supporting the presently suggested theory such that the melt break up takes place on the equator of the moving melt inside a surrounding fluid [27]. To determine this critical condition that the hydrodynamic disruptive forces exceeds the stabilizing surface tension forces, Weber number (the ratio of the destabilizing inertia force to the stabilizing surface tension force) should be involved. An empirical equation giving the critical We number was proposed by Brodkey [31] for the gas liquid systems (Equation 4.3).

$$We_{crit} = 6\left(1 + 1.077 * On^{1.6}\right) \tag{4.3}$$

Where, $On = \mu_{melt} \Big/ \left(\rho_{melt}.2.r_m.\sigma_{melt}\right)^{0.5}$ (Ohnesorge number) and $We = \rho.u_1^2\ r_{melt} \Big/ \sigma_{melt}$ (Weber number)

Dynamic viscosity and surface tension are represented as μ and σ, respectively. Similar correlations [32, 33] suggested for the liquid-liquid (oil drops surrounded by water) mediums show that *We* number is the same both for liquid-liquid systems and gas liquid systems. According to Equation (4.3), after a certain value of relative velocity, the critical *We* will be exceeded and the fragmentation process will start. When the values of *We* and

$$u_1^2 = \frac{6.\sigma_{melt}}{\rho_{coolant}.r_m}\left[1+1.077\left(\frac{\mu_{melt}}{(\rho_{melt}.2r_m.\sigma_{melt})^{0.5}}\right)^{1.6}\right] \tag{4.4}$$

On are placed in Equation (4.3), Equation (4.4) is obtained. From Equation (4.4), it is seen that the magnitude of u_1 depends on some physical properties of the moving melt (droplet) and the surrounding medium. If this u_1 value is inserted in Equation (4.2) suggested by the present author, the critical pressure distribution can be obtained for every point on the surface of the spherical melt droplet depending on φ, θ and r_m. As is explained in the previous chapter, acceleration caused disturbance can result in film collapse in other locations. Because the time between the two subsequent film collapses is very small, the motion of the melt droplet is a vibration.

The size of the melt droplet is very important for the fragmentation process caused by the inertial forces. As a result of fragmentation, the diameter of the melt droplet becomes smaller and the inertial forces can no longer overcome the stabilizing surface tension forces. In brief, surface tension forces stop the fragmentation process when the melt droplet size becomes small enough. In the following chapters, it has been indicated that the critical debris diameter (minimum diameter until the fragmentation process continues) is about $10\,\mu m$ for the large-scale steam explosion experiments performed in the ALPHA facility of Japan Atomic Energy Research Institute.

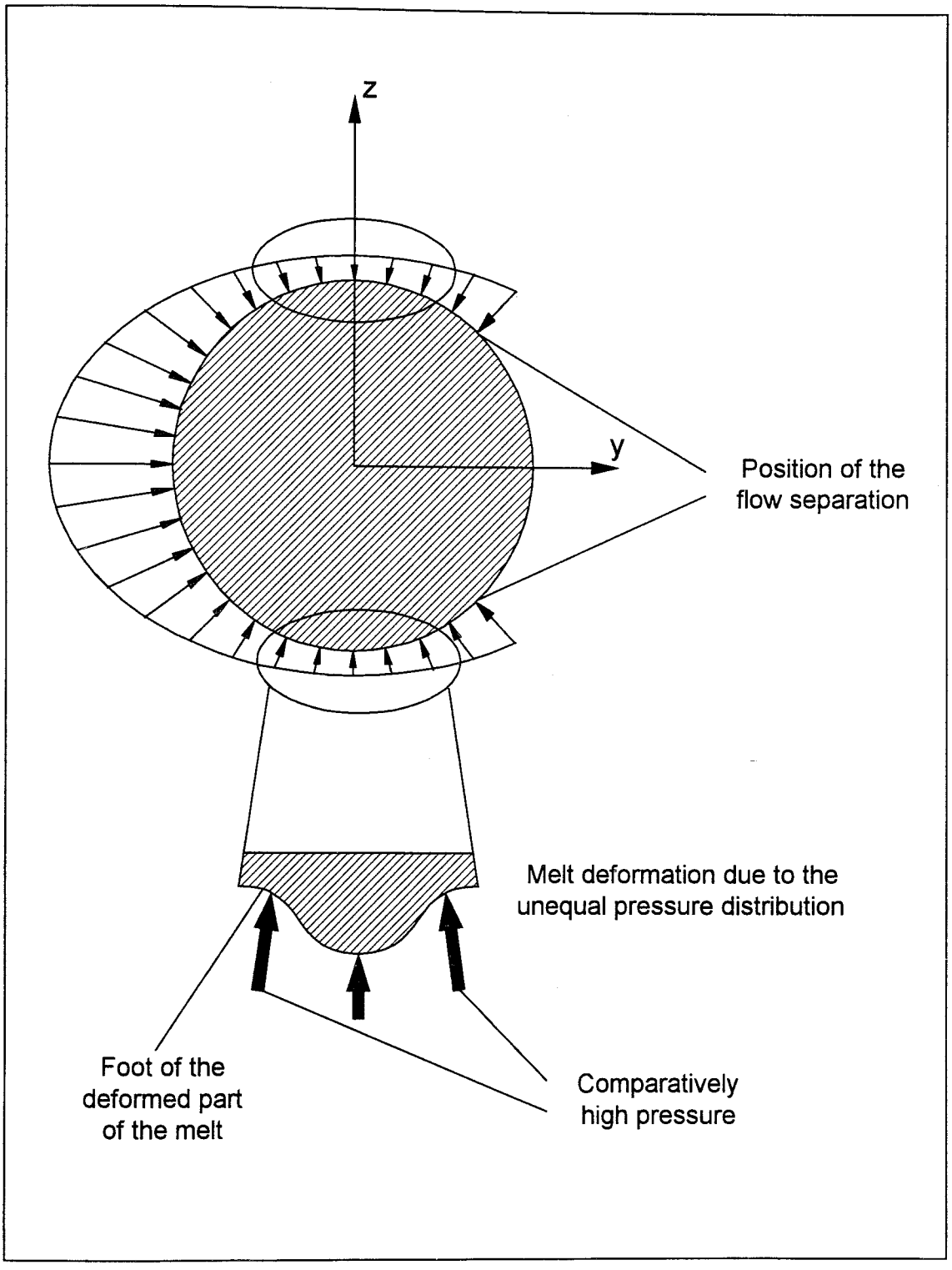

Figure 4.3. Deformation of the melt due to the uneven pressure distribution

4.2. Propulsive Force as a Result of Triggering

As is explained in the previous chapter qualitatively, the author believes that the coolant does not have enough time to penetrate into the melt, if the melt temperature is above the spontaneous nucleation temperature of the coolant, which is a necessary condition for triggering. Instead, the coolant will evaporate creating a propulsive force that causes the melt to move in the surrounding coolant. In the first part of this chapter, a theory giving the hydrodynamic pressure distribution on the melt has been proposed. However the pressure forces applied on the moving melt by the surrounding coolant are not the only forces causing the melt to be deformed and broken up. Since the melt particle is not a solid body, the propulsive forces (due to the local explosive steam production) will also cause the melt to be deformed. As a result of triggering (according to author, explosive local evaporation of the coolant), some amount of steam will penetrate into the melt. Thermal theory, present in the literature, assumes that coolant (in the form of liquid) jet penetrates into the melt; and sudden evaporation of the coolant inside the melt will cause it to be broken up. Whereas, according to the theory suggested by the author, the steam penetrates into the melt and applies a propulsive force on the melt (Figure 4.4.). The penetration of steam jet into the melt creates a mushroom type steam bubble inside the melt. To simplify the mathematical model, this mushroom type bubble will be assumed as spherical having a radius r_b. The average radius of the steam jet at the root of the mushroom type steam bubble is r_j. The number of the steam jets is n. The absolute velocity of the steam bubble in the x direction and the velocity of the steam jet are u_b and u_j, respectively. Jet penetration distance is X_j (except the steam bubble). It is assumed that the steam jet penetrating into the melt has a parabolic velocity profile (Figure 4.4.). When $r = 0$, u_j is maximum. When $r = r_j$, $u_j = u_1$ (no slip condition). For an incompressible flow, from the conservation of mass:

$$\frac{dM_{melt}}{dt} = \sum_{1}^{n} 2\pi\rho_{jn} \int_{0}^{r_{jn}} (u_{jn} - u_1) r dr \tag{4.5}$$

ρ_j represents the density of the steam jet. In Equation (4.5), it is assumed that the time rate of change of mass of the melt droplet is caused only by the steam penetration into the melt.

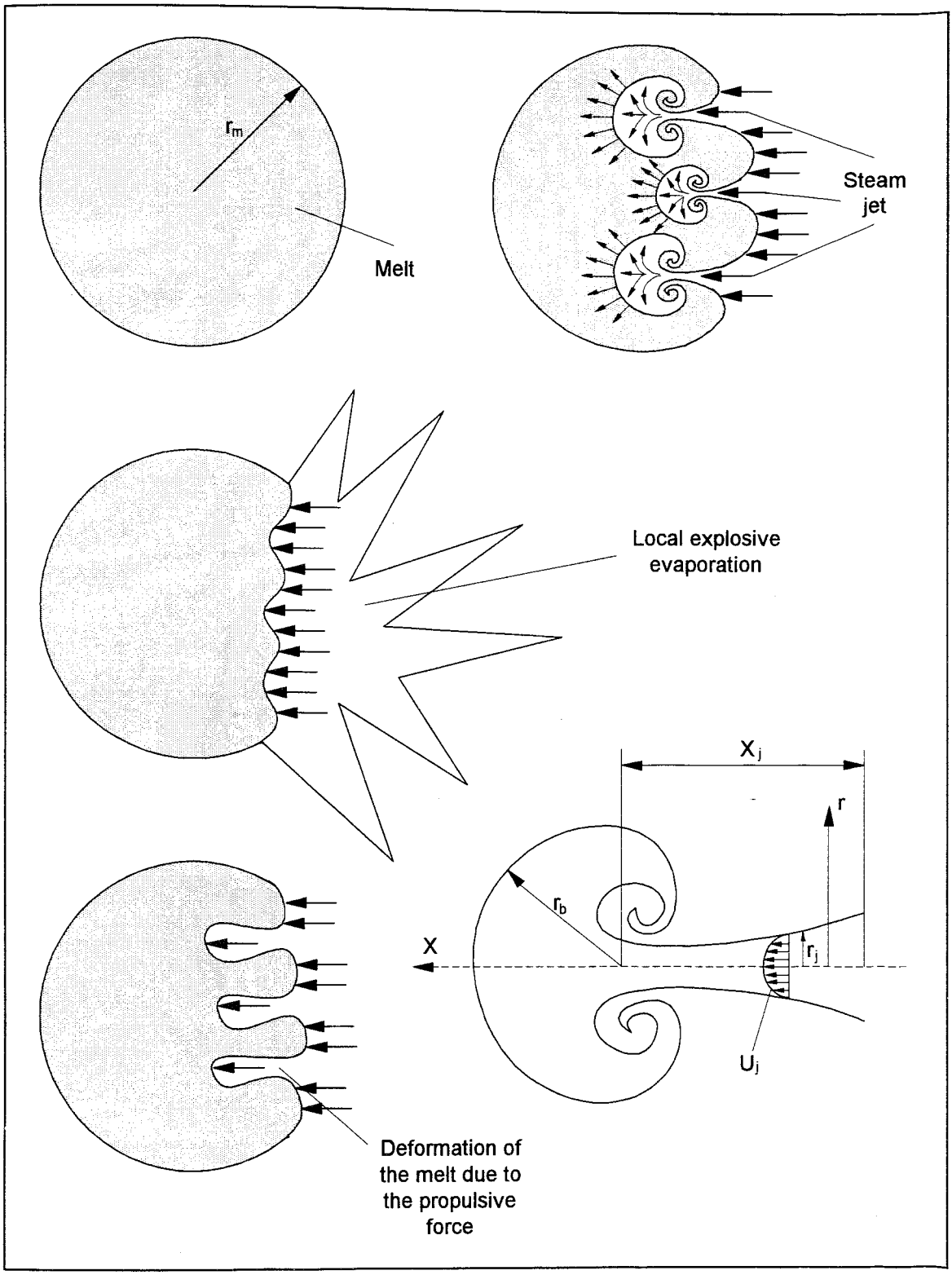

Figure 4.4. Penetration of steam jets into the melt

In another word, Equation (4.5) is written for the time period between the occurrence of triggering and just before the critical velocity is reached. Therefore, the time rate of change of mass of the melt droplet due to the fragmentation has not been taken into consideration. M_{melt} is equal to the actual mass of the melt droplet + the mass of the steam penetrating into the melt; so, dM_{melt}/dt is equal to the time rate of change of steam mass penetrating into the melt. From the conservation of momentum:

$$\frac{d(M_{melt}u_1)}{dt} = \sum_1^n \left(C_{dmb}\,\tfrac{1}{2}\rho_{melt}(u_{bn}-u_1)^2\pi.r_{bn}^2 + \tau \left.\frac{d(u_{jn}-u_1)}{dr}\right|_{r=r_{jn}} X_{jn}\,2\pi r_{jn} \right) + P_{st}\left(\pi.r_m^2 - \sum_1^n \pi r_{jn}^2\right) - C_{dcm}\,\tfrac{1}{2}\rho_{coolant}.u_1^2.\pi.r_m^2 \tag{4.6}$$

Equation (4.6) can be written. τ is the shear stress between the steam jet and the melt. P_{st} is the pressure of the steam due to the local explosive steam production. C_{dmb} is the drag coefficient between the mushroom type steam bubble and the melt in which the steam bubble moves. C_{dcm} is the drag coefficient between the spherical melt droplet and the surrounding coolant. The first term on the right hand side of Equation (4.6) shows the drag force acting on the melt by the mushroom type steam bubble that moves inside the melt droplet. The second term indicates the shear stress caused propulsive force at the root of the mushroom type bubble due to the relative velocity between the melt droplet and the steam jet penetrating into the melt. The third term represents the propulsive force by the pressure due to the explosive steam production. The last term on the right hand side of Equation (4.6) gives the drag force acting on the moving melt by the surrounding medium (coolant). Since the drag force applied by the coolant is in the negative direction of the melt velocity, minus sign is employed. The left hand side of Equation (4.6) can be written as:

$$\frac{d(M_{melt}u_1)}{dt} = u_1\frac{dM_{melt}}{dt} + M_{melt}\frac{du_1}{dt} \tag{4.7}$$

If Equation (4.7) and (4.5) is placed in Equation (4.6):

$$u_1 \sum_1^n 2\pi\rho_{jn} \int_0^{r_{jn}} (u_{jn} - u_1) r dr + \rho_{melt} \frac{4}{3}\pi r_m^3 \frac{du_1}{dt} =$$
$$\sum_1^n \left(C_{dmb} \tfrac{1}{2} \rho_{melt} (u_{bn} - u_1)^2 \pi . r_{bn}^2 + \tau \frac{d(u_{jn} - u_1)}{dt} \frac{dt}{dr}\bigg|_{r=r_{jn}} X_{jn} 2\pi r_{jn} \right) \qquad (4.8)$$
$$+ P_{st} . \left(\pi . r_m^2 - \sum_1^n \pi r_{jn}^2 \right) - C_{dcm} \tfrac{1}{2} \rho_{coolant} . u_1^2 . \pi . r_m^2$$

After the triggering the melt particle will start to move in the opposite direction of where the explosive steam production takes place. Under the effect of the propulsive force, the speed of the melt will increase first; and then will decrease due to the friction (drag) force the coolant applies on the melt. The maximum u_1 value is reached when $du_1/dt = 0$. Therefore, when $du_1/dt = 0$ is inserted in Equation (4.8), Equation (4.9) is obtained. In Equation (4.9), u_1 is the critical velocity, which is determined by the physical properties of the melt and the coolant.

$$u_1 \sum_1^n 2\pi\rho_{jn} \int_0^{r_{jn}} (u_{jn} - u_1) r dr =$$
$$\sum_1^n \left(C_{dmb} \tfrac{1}{2} \rho_{melt} (u_{bn} - u_1)^2 \pi . r_{bn}^2 + \tau \frac{d(u_{jn})}{dr}\bigg|_{r=r_{jn}} X_{jn} 2\pi r_{jn} \right) \qquad (4.9)$$
$$+ P_{st} . \left(\pi . r_m^2 - \sum_1^n \pi r_{jn}^2 \right) - C_{dcm} \tfrac{1}{2} \rho_{coolant} . u_1^2 . \pi . r_m^2$$

The value of u_1 determined by means of the empirical Equation (4.4) can be written in Equation (4.9). Equation (4.9) gives a relation between P_{st} and several physical parameters of the interaction region consisting of melt, coolant and steam.

In addition to those equations, conservation of energy equation should also be employed to obtain a relation between the heat transfer coefficient and the other physical parameters of the interaction region.

$$\frac{d\left[\rho_{melt}\frac{4}{3}.\pi.r_m^3\left(e+\frac{u_1^2}{2}\right)\right]}{dt}=$$

$$\sum_1^n\left(C_{dmb}\frac{1}{2}\rho_{melt}(u_{bn}-u_1)^2\pi.r_{bn}^2u_1+u_1\tau\frac{d(u_{jn}-u_1)}{dt}\frac{dt}{dr}\bigg|_{r=r_{jn}}X_{jn}2\pi r_{jn}\right) \tag{4.10}$$

$$+P_{st}\left(\pi.r_m^2-\sum_1^n\pi r_{jn}^2\right)u_1-C_{dcm}\frac{1}{2}\rho_{coolant}.u_1^3.\pi.r_m^2$$

$$-\left(4\pi.r_m^2+\sum_1^n\left(4\pi.r_{bn}^2+X_{jn}.2.\pi.r_{jn}\right)\right).h_{total}\Delta T$$

As is known well, in the premixing stage, heat is transferred from the molten droplet to the surrounding coolant by means of film boiling and radiation. If the heat transfer by radiation would have been high enough to cause the surrounding volatile coolant to evaporate fast enough, as in the case of expansion stage, the complicated stages of steam explosion such as triggering and propagation would be eliminated i.e., the steam explosion would occur just in the premixing stage. However, this is not the actual case. Therefore, the author considers that the heat transfer rate by means of radiation is smaller than the convective heat transfer rate.If $h_{radiation}\angle h_{convection}$, Bromley [34] suggested that:

$$h_{total}=h_{convection}+\frac{3}{4}h_{radiation} \tag{4.11}$$

The term on the left hand side of Equation (4.10) indicates the time rate of change of the sum of the total internal and kinetic energy of the melt, which is assumed as spherical. The first term on the right hand side of Equation (4.10) represents the work done on the melt per unit time by the drag force due to the moving steam bubble inside the melt. The second term is the work done on the melt per unit time by the shear stress due to the relative velocity gradient between the melt and the steam penetrating into the melt. Where n is the number of the steam jets. The third term shows the work done on the melt per unit time by the propulsive force due to the small-scale explosive steam production. To calculate this term, P_{st} should be multiplied by the projected area on the plane that is perpendicular to the motion. Since the melt is assumed as spherical, this area is a circle having a radius r_m. The cross sectional area of each steam jet should be subtracted from this area. The fourth term is the work done by the surrounding coolant due to the drag force caused by the relative velocity of the moving melt.

Because the drag force is in the opposite direction of the velocity, a minus sign should be used in front of this term. The last term indicates the heat transfer by means of convection and radiation. The heat transfer area includes not only the outside area of the melt but also the inside area where the steam jets contact the melt. Since the heat is transferred from the melt to the surrounding coolant, a minus sign should be used.

At this stage it should be pointed out that the model developed by the author substantially differs from the phenomenological model developed by Ciccarelli and Frost [29]. Very briefly, the phenomenological model suggested in reference [29] can be summarized that local steam production just after the collapse of the steam film creates some craters forming tiny filaments, which are broken into small fragments and move away from the melt in the expanding steam medium. According to reference [29], after the steam film is destabilized and moves toward the melt again, small fragments continue to go away from the melt because of their high inertia. Whereas, according to the model suggested in this Ph.D. study, fragmentation is mainly caused by the hydrodynamic pressure distribution at the equator of the moving melt in the surrounding coolant. The author also believes that at the final stage of fragmentation, continuously growing mushroom type steam bubbles will also cause the remaining melt to be broken up.

According to the theory suggested by the author, after the film collapse, violent boiling or explosive local steam production is one of the necessary conditions to have a propulsive force leading to hydrodynamic fragmentation. If the ambient pressure is increased, it will be more difficult to obtain violent boiling or explosive local steam production at the same temperature conditions. However, this result should not be concluded as high ambient pressure suppresses the steam explosions. The correct conclusion is high ambient pressure makes the triggering process to become more difficult. In another words, a stronger pressure pulse can be necessary to initiate the triggering process. This result is in quite good agreement with the large-scale steam explosion experiments done in the ALPHA facility of Japan Atomic Energy Research Institute (There is only one exceptional experiment) [35]. Steam explosion occurred in 13 experiments out of 19 experiments done under the condition of 0.1 MPa ambient pressure. Whereas, steam explosion was observed only in one experiment out of four done under the condition of elevated ambient pressure. More specifically, steam explosion has not been observed in the three experiments for 1, 1.6 and 1.6 MPa ambient pressures. Only the experiment done under the 0.5 MPa ambient pressure resulted in explosion [35].

4.3. Solution of the Model Conservation Equations

Using the Equations (4.9) and (4.10), following equation can be obtained. When the

$$u_1.\sum_1^n 2.\pi\rho_{jn}\int_0^{r_{jn}}(u_{jn}-u_1)rdr=\frac{1}{u_1}\frac{d\left[\rho_{melt}\frac{4}{3}\pi.r_m^3(e+{u_1^2}/{2})\right]}{dt}+$$
$$+\frac{1}{u_1}\left(4.\pi.r_m^2+\sum_1^n\left(4.\pi.r_{bn}^2+X_{jn}.2.\pi.r_{jn}\right)\right)h_{total}.\Delta T \qquad (4.12)$$

critical velocity is reached, u_1 is maximum and $\frac{du_1}{dt}=0$. Therefore, Equation (4.12) can be written in the following form.

$$u_1.\sum_1^n 2.\pi\rho_{jn}\int_0^{r_{jn}}(u_{jn}-u_1)rdr=\frac{1}{u_1}\rho_{melt}\frac{4}{3}\pi.r_m^3\frac{de}{dt}+$$
$$+\frac{1}{u_1}\left(4.\pi.r_m^2+\sum_1^n\left(4.\pi.r_{bn}^2+X_{jn}.2.\pi.r_{jn}\right)\right)h_{total}.\Delta T \qquad (4.13)$$

If Figure 4.4. is taken into consideration, it is seen that the time rate of change of mass of the steam penetrating into the melt is equal to the time rate of change of volume of the mushroom type bubble multiplied by the density of the penetrating steam. Therefore,

$$\sum_1^n 2.\pi\rho_{jn}\int_0^{r_{jn}}(u_{jn}-u_1)rdr=\sum_1^n\rho_{jn}\frac{d}{dt}\left(\frac{4}{3}\pi.r_{bn}^3\right)=\sum_1^n\rho_{jn}\frac{4}{3}\pi.3.r_{bn}^2\frac{dr_{bn}}{dt} \qquad (4.14)$$

Equation (4.14) can be written. Beside this, the time derivative of the internal energy can be written as:

$$\left(\frac{de}{dt}\right)=\frac{d(c.T)}{dt} \qquad (4.15)$$

If those values are inserted in Equation (4.13), Equation (4.16) is obtained.

$$u_1.\sum_1^n \rho_{jn}\frac{4}{3}\pi.3.r_{bn}^2\frac{dr_{bn}}{dt}=\frac{1}{u_1}\rho_{melt}\frac{4}{3}\pi.r_m^3 c\frac{dT}{dt}+ \\ +\frac{1}{u_1}\left(4.\pi.r_m^2+\sum_1^n\left(4.\pi.r_{bn}^2+X_{jn}.2.\pi.r_{jn}\right)\right)h_{total}.\Delta T \tag{4.16}$$

The probability that the coolant comes into contact with the melt at several points exactly at the same time is low. Since the melt temperature is above the spontaneous nucleation temperature as one of the necessary conditions to have a steam explosion, the coolant will almost instantly evaporate when it comes into contact with the melt. To simplify the equation, it is assumed that during this very small time interval (evaporation time), there is no other contact of coolant with the melt at any other location. In another words, in the summation term, "n" is accepted as one. Since r_j is much smaller than r_m and r_b, the term that is multiplied by r_j is neglected. When Equation (4.16) is rearranged, Equation (4.17)

$$u_1^2.\rho_j.r_b^2\frac{dr_b}{dt}=\rho_{melt}\frac{1}{3}.r_m^3.c\frac{dT}{dt}+\left(r_m^2+r_b^2\right)h_{total}.\Delta T \tag{4.17}$$

is obtained. u_1 can be obtained from Equation (4.4). In Equation (4.4), surface tension (σ_{melt}) and the viscosity (μ_{melt}) of the melt obtained by thermite reaction of iron oxide and aluminum are not known. For the pure molten aluminum, surface tension varies from 0.36 to 0.683 N/m depending on the measurement method [36]. For the melt used in ALPHA experiments, $\sigma = 0.5$ N/m can be a reasonable assumption [private communication with Dr. Moriyama]. For the viscosity, following empirical relation suggested by Blomguist [37] is used.

$$\mu=\exp\left(\frac{11448}{T}-8.2734\right) \tag{4.18}$$

In this correlation, the units of μ and T are [Pa.s] and [K], respectively. For the ALPHA experiments, the surface temperature of the melt after the reaction is 2700 K [35]. Using the above equation μ is calculated as $9.26\text{x}10^{-5}$ [Pa.s]. The density of the melt is $3.62\text{x}10^3$ kg/m^3 [35]. In the real experimental conditions, the mass of the melt parts are different from one another for the premixing stage. However, it is a reasonable approximation to accept that

melt consists of spherical particles having 1 cm average diameter (r_m=0.5 cm). Using all those values in Equation (4.4), critical velocity u_1 can be calculated as 0.775 m/s. It should be emphasized that the motion of the melt droplet is a vibration due to the subsequent film collapses in the several other regions (Figure 3.3. d and f). Therefore, a bulk motion or a considerable displacement of the melt droplet is out of the question at the triggering stage.

Integrating both sides of Equation (4.17), Equation (4.19) can be obtained. Assuming that the density of the penetrating steam is homogeneous everywhere in the melt,

$$u_1^2 \rho_j \int r_b^2 dr_b = \rho_{melt} \frac{1}{3} r_m^3 c \int dT + r_m^2 h_{total} \Delta T \int dt + h_{total} \Delta T \int r_b^2 dt \qquad (4.19)$$

r_b can be written as a function of time (t). Where $\dot{m}_{steam}$ is the time rate of change of

$$\rho_j \frac{4}{3} \pi . r_b^3 = t . \dot{m}_{steam} \qquad (4.20)$$

steam mass penetrating into the melt. When $t = 0$, $r_b = 0$. At the end of the triggering stage, the volume of the steam penetrating into the melt reaches a certain value such that the melt is fragmented. It is assumed that when $r_b = r_m / 2$ the melt is deformed and divided into its pieces. At the end of the premixing stage, it is reasonable to assume that the average melt radius is 0.5 cm. Since triggering takes place in about 0.1 ms, the integration should be carried out between the time limits from 0 to 0.1 ms. Inserting those values in Equation (4.20):

$$\frac{\dot{m}_{steam}}{\rho_j \frac{4}{3} \pi} = 0.00015625 \qquad (4.21)$$

$$r_b = 0.05386 . t^{1/3} \qquad (4.22)$$

Equation (4.22) is inserted in the last term of equation (4.19). At the instant of fine fragmentation, it is conventionally accepted that the heat is transferred from the melt to the coolant in a very short time such that melt, water and the steam have the same temperature in the interaction region just after the triggering. During the ALPHA experiments, just after the fine fragmentation, it is determined experimentally that the temperature of the water suddenly rises to about 1500K. Therefore, this temperature will be used as the temperature of the melt just after the interaction. Since the initial surface temperature of the melt is 2700K, the integration limits of the first term on the right hand side of Equation (4.19) should be taken from 2700K to 1500K. In equation (4.19), integration limits concerning the time should be the same time interval in which the triggering takes place, i.e. from 0 to $0.1\text{x}10^{-3}$s. During the ALPHA experiments the pressure in the water pool rises instantly up to about 25 MPa. Technically, it is impossible to measure the pressure just at the location of the triggering, which is previously unknown. Making an approximation, steam density (13,601 kg/m^3), at 25 MPa pressure and at 1500K temperature, has been taken as the density of the steam that penetrates into the melt. Specific heat capacity and the density of the melt (iron alumina thermite mixture) used in ALPHA experiments are $c = 0.96\text{x}10^3 J/kg$ and $\rho_{melt} = 3.62\text{x}10^3 kg/m^3$ [35]. Initial water temperature, before the melt is dropped into the pool is about 300K. Hence, $\Delta T = 2700 - 300 = 2400$. If all those values are inserted in Equation (4.19), heat transfer coefficient (h_{total}) can be calculated as $25.1\text{x}10^6 W.m^{-2}K^{-1}$

4.4. Evaluation of the Heat Transfer Coefficient

Heat transfer coefficient is one of the most important parameters in modeling the steam explosion phenomenon. Unfortunately, because of the uncertainties and experimental difficulties, it is almost impossible to determine the exact value for a given location and time during the fragmentation process. The sources of the experimental difficulties are the very small time scales (millisecond), high pressures and temperatures. Available experimental data about the heat transfer coefficient are rough and time averaged values during the fragmentation process. According to a review of the literature, the time-averaged value of the heat transfer coefficient is in the range of $10^5 - 10^6 Wm^{-2}K^{-1}$ when the heat transfer is to a high-density fluid [16]. However, there is a significant uncertainty concerning the accuracy of this range [38, 39]. Especially, for the two-phase flow (this is the case for the steam explosion

phenomenon), heat transfer coefficient highly depends on whether the fragments are in contact with the steam or water phase. When the fragments are in contact with the steam, the time averaged value of the heat transfer coefficient is about $10^3 Wm^{-2}K^{-1}$. This value corresponds to the film-boiling regime, if the melt temperature is about 3000 K. When film collapse occurs due to the decreasing melt temperature, the heat transfer coefficient becomes about $10^6 Wm^{-2}K^{-1}$ for the enhanced boiling regime [38]. Although the heat transfer area increases as a result of fine fragmentation, the heat transfer rate necessary for an explosive steam production per unit time is much greater than the steam production observed during the steady nucleate boiling regime [22].

According to the heat transfer model developed by Fletcher and Thyagaraja [40], heat transfer coefficient between the melt and the coolant can be $10^7 Wm^{-2}K^{-1}$, even for the high void fractions such as 90%. They indicated that if the heat transfer coefficient was $10^7 Wm^{-2}K^{-1}$, the propagation shock wave occurred for a spherical geometry. Whereas, it did not occur for a spherical geometry, if the heat transfer coefficient is reduced to $10^5 Wm^{-2}K^{-1}$. Heat transfer coefficient at the surface of UO_2 particles in contact with water is about $10^5 Wm^{-2}K^{-1}$. If the surface heat transfer coefficient exceeds about $10^7 Wm^{-2}K^{-1}$, it becomes diffusivity limited for UO_2 particles having 250 μm diameter [41]. Average heat transfer coefficient of $10^6 Wm^{-2}K^{-1}$ has been obtained for a time interval of 100 μs in the experiments with pulse-heated wires submerged in a water pool [42].

The heat transfer coefficient $25.1x10^6 Wm^{-2}K^{-1}$ calculated by the author is the maximum value, not the time averaged value during the fragmentation process. Heat transfer by radiation is also included in the convection term. Model equations have been solved for the instant when the fragmentation process starts, i.e. the critical velocity is reached. Beside the uncertainties and inevitable assumptions made in the solution of the model equations, the facts and comments mentioned above are the reasons that the calculated heat transfer coefficient by the author is bigger than the one present in the literature.

Since the pressure wave is sustained by the heat transfer from the melt to the coolant, it is very important to determine heat transfer coefficient. Before the shock wave reaches an unfragmented melt drop, heat transfer is maintained by means of radiation and film boiling.

At this stage (coarse mixing or premixing) heat transfer rate is low; almost negligible compared to that in the triggering stage. Just behind the shock wave or in the shock layer where the differential velocities force the melt to be broken-up, the flow field is very complicated due to the uncertainties. That is why many researchers assumed that fragmented melt equilibrate its temperature instantaneously with the surrounding coolant [16]. The same simplification has also been done in the suggested model by the present author. It is important to remember that the maximum heat transfer coefficient found by the present author may not correspond to the time when the heat transfer rate reaches its peak during the triggering and fragmentation of a melt droplet. Because the heat transfer coefficient was calculated for the very small time interval between the steam film collapse and the beginning of fragmentation, heat transfer by means of area enlargement does not contribute to the heat transfer rate in this time range.

4.5. Uncertainty Analysis of the Heat Transfer Coefficient

In the calculation of the heat transfer coefficient (h), it has been assumed that the diameter of the penetrating steam bubble is $r_b = r_m/2 = 0.005/2 = 0.0025m$. In order to determine the uncertainty in (h) due to this assumption, heat transfer coefficient (h) has been calculated for several r_b values; i.e., ($r_b = r_m/2$, $r_b = r_m/3$, $r_b = r_m/4$ and $r_b = r_m/5$). The corresponding (h) values are $25.1x10^6$, $27.1x10^6$, $27.9x10^6$ and $28.2x10^6 Wm^{-2}K^{-1}$, respectively. In other words, 25 % increase in r_b (from $r_b = r_m/5$ to $r_b = r_m/4$) leads to 1,4 % decrease in (h). 32,8 % increase in r_b (from $r_b = r_m/4$ to $r_b = r_m/3$) causes the (h) to decrease 2,9 %. If r_b is increased by 50,6 % (from $r_b = r_m/3$ to $r_b = r_m/2$), (h) will decrease about 7 %. Even for a big uncertainty range concerning r_b, such as 150 % increase (from $r_b = r_m/5$ to $r_b = r_m/2$), the heat transfer coefficient (h) will decrease only about 10,6 %.

Outer surface area enlargement of the melt due to the penetration of steam is 0.4 % for $r_b = r_m/5$. For only exaggerated values of r_b, surface enlargement of the melt can be an important parameter that affects the magnitude of (h). Therefore, it has not been taken into consideration in the calculation of (h).

To understand the effect of melt radius on the heat transfer coefficient, (h) has been calculated for a variety of (r_m) values. Some examples are presented here: When the radius of melt is increased 50 %, the necessary heat transfer coefficient, which leads to an explosion, increases about 50,2 %. If the radius of the melt is doubled, the increase in the heat transfer coefficient will be 100,4 %. Similarly, 50 % decrease in the melt radius corresponds 49,8 % decrease in the heat transfer coefficient. Those numerical results indicate that when the radius of the melt increases, the necessary heat transfer rate should increase to obtain a small-scale steam explosion. For the smaller values of melt radius, comparatively smaller heat transfer rates can be enough to trigger the explosion. In other words, the degree of the melt break-up in the premixing stage is important in determining the percentage of the melt that contributes to the large-scale steam explosion. Indeed, comparatively finer melt-break-up in the premixing stage, as in the case of melt and coolant injection modes, leads to more energetic steam explosions. This result is in good agreement with the widely accepted idea. Of course, some exceptional triggering mechanisms, such as coolant entrapment between the bulk of the molten metal and the bottom of the container, should be excluded.

The effect of penetrating steam density on the heat transfer coefficient (h) is negligible; i.e., 100 % decrease in the penetrating steam density can cause the heat transfer coefficient to decrease less than 0.001 %. It is obvious that the most influential parameter on the heat transfer coefficient is the triggering time. The heat transfer coefficient is almost inversely proportional to the triggering time; i.e., 100 % increase in the triggering time, can lead to 50 % decrease in the heat transfer coefficient for a certain geometry and experimental conditions. This result is quite reasonable. Because the amount of heat transfer necessary to get a small-scale steam explosion (triggering) is fixed during a certain triggering time, it is evident that the heat transfer coefficient should be inversely proportional to the triggering time. Some single drop experiments, such as the one done in the Central Research Institute of Electric Power Industry, Japan, revealed that the triggering time is about 0.1 ms [43]. Therefore, 0.1 ms was used as the triggering time in the calculation of (h).

4.6. Formation of the Propagation Wave

As a result of triggering, fast local steam production can create a pressure pulse in the interaction region. If the steam production is fast enough, such that the expansion velocity of the steam water interface is higher than the speed of sound, a shock wave is initiated. Visual evaluation of the ALPHA large-scale steam explosion data [35] revealed that the propagation wave cannot continue easily in the regions where the void fraction is high. This shock wave mainly propagates in the water. Therefore, to obtain a shock wave, the speed of the expanding steam-water boundary should be greater than the speed of sound in the water. Speed of sound in water at 300 K temperature is about 1450 m/s. Heat transfer rate from the melt to the water is:

$$q = h.A.\Delta T \tag{4.23}$$

$$q = h.4r_m^2\pi.(2700-300) \tag{4.24}$$

$$q = 25.10^6.4.(0.005)^2.\pi.2400 \tag{4.25}$$

$$q = 18.85x10^6 W \tag{4.26}$$

Heat of vaporization: $h_{fg} = 2438000\ {}^{J}/_{kg}$

$$\frac{d\left(\frac{4}{3}\pi.r^3 - \frac{4}{3}\pi.(0.005)^3\right).\rho}{dt} = \frac{q}{h_{fg}} \tag{4.27}$$

$$\frac{4}{3}\pi.3r^2.\frac{dr}{dt} = \frac{q}{\rho.h_{fg}} \tag{4.28}$$

$$u = \left.\frac{dr}{dt}\right|_{r=r_m} = \frac{q}{4.\pi.r^2.\rho.h_{fg}} \tag{4.29}$$

Then, u is found as $u = 1809\ {}^{m}/_{s}$.

Above calculated velocity demonstrates that the heat transfer coefficient $25.1.10^6 Wm^{-2}K^{-1}$ is just high enough to obtain a shock wave for the conditions used in the solution of the model equations. When $r = r_m = 0.005m$, the radius of the spherical steam-water interface is the minimum. The minimum radius r_m corresponds to the maximum velocity of the spherical steam-water interface. While the radius increases, the velocity of the interface boundary decreases. Until the velocity of the interface boundary becomes equal to the speed of sound, it sustains the shock wave. Thus:

$$u = \frac{dr}{dt} = \frac{q}{4.\pi.r^2.\rho.h_{fg}} = 1450m \tag{4.30}$$

The corresponding r value can be obtained as 0.0056m. The result obtained by solving the model equations indicates that fast steam production is high enough to create a shock wave; however, it sustains the shock wave for only about 0.6 mm. This outcome is fairly reasonable, because additional steam production as a consequence of fragmentation and area enlargement has not been taken into consideration in the model equations. Of course, additional steam production due to the area enlargement will cause the propagation shock wave to be sustained for a further distance (Figure 4.5.).

. The speed of the expanding steam-water boundary is directly proportional to the heat transfer coefficient (h). The heat transfer coefficient uncertainty analysis done in the previous subsection will directly affect the velocity of the steam-water boundary. When the bigger (h) values are used, the velocity of the expanding steam-water interface becomes higher. Among the several heat transfer coefficients corresponding to different r_b (radius of the penetrating steam bubble) values, the smallest one ($25.1x10^6 Wm^{-2}K^{-1}$) has been used for the above calculation of the interface velocity. Even the smallest one is high enough to obtain a shock wave, which is one of the necessary conditions to have a large-scale steam explosion.

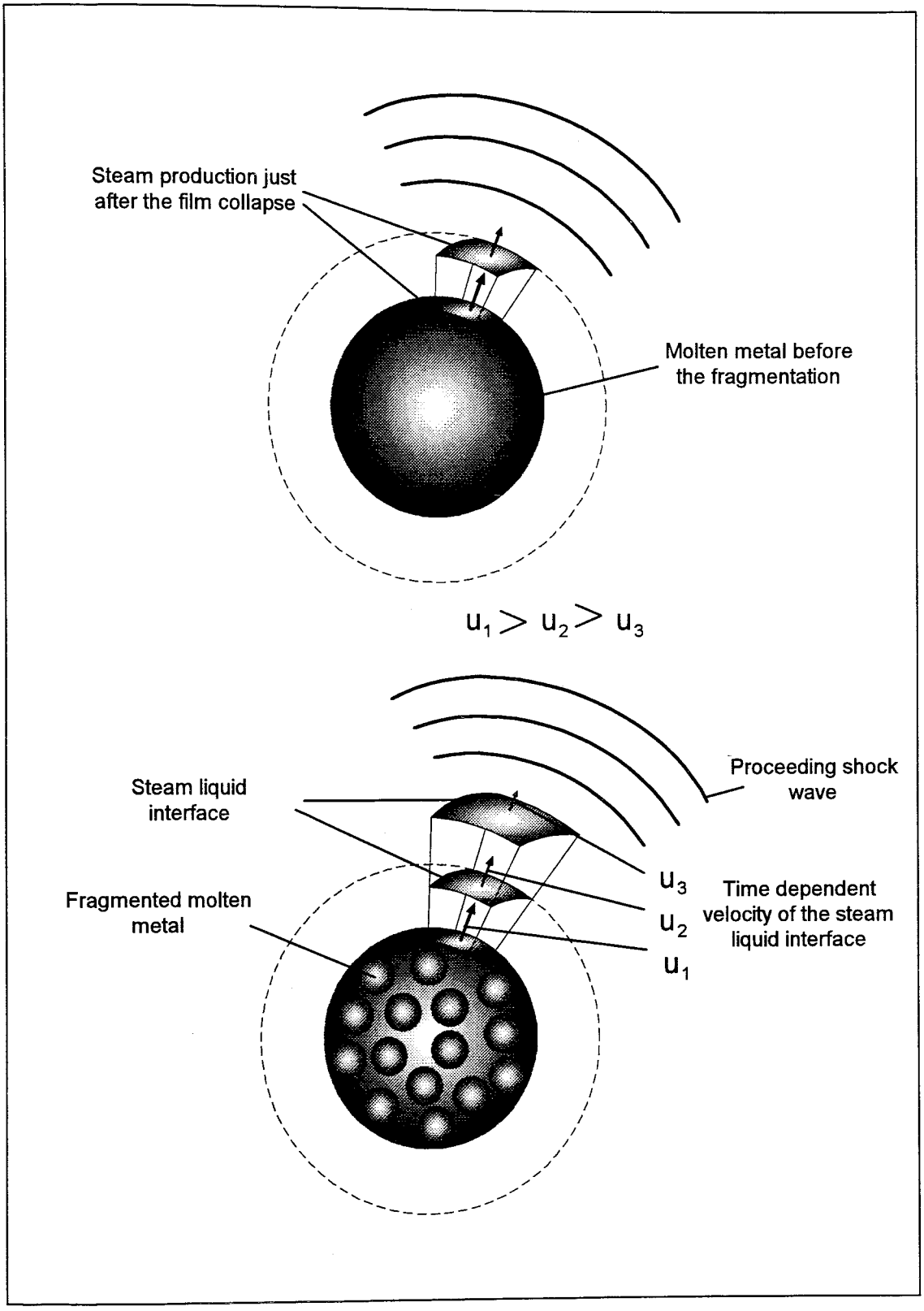

Figure 4.5. A sketch of the propagation wave

5. EXPERIMENTAL APPARATUS

Basic properties of the ALPHA experimental facility of Japan Atomic Energy Research Institute are seen in Figure 5.1. The melt generated by a thermite reaction with iron oxide and aluminum (before the reaction Iron oxide 78, Aluminum 22; after the reaction Iron 58, Aluminum 42) in the melt generator is dropped in to the water pool made of acrylic resin. The volume, the height and the inner diameter of the ALPHA containment vessel are $50\,m^3$, $5.7\,m$ and $3.9\,m$, respectively. Its maximum pressure is 2MPa and the maximum melt generation capacity is 100kg. It is possible to pressurize the containment vessel by nitrogen. The facility has several windows to observe the experiments.

Two types of melt dropping systems have been conducted. In the early large-scale steam explosion experiments carried out in ALPHA, the two thermite layers -upper and lower- have been separated by 4 kg Magnesium Oxide (MgO) powder, which acts as an insulator. The two layers of thermite and a layer of MgO have been placed on a glass plate. Lower layer thermite is electrically ignited after all of the upper layer thermite melts. High temperature generated by the exothermic thermite reaction in the lower layer causes the glass plate to be broken. Subsequently, all the melt and MgO drop into the water pool through a 200 mm diameter orifice.

Since MgO can affect the breakup phenomenon in the premixing stage, two layers of 3 mm thick carbon steel plates have been used instead of MgO for the experiments after 1993. The reaction in the upper layer takes 12s; and, the total time period between the initiation of the thermite reaction and the release of the melt mass is 20 s. No external trigger was used in any of the tests.

Three different sizes of transparent water pools made of acrylic panels have been used for the experiments. The smallest one has a depth of 138cm and a square cross-section with one side 45cm. The depth and the length of one side of the square cross-section of the medium water pool are 112 cm and 63 cm, respectively. The largest pool has a 120 cm depth and 88 X 88 cm cross-section.

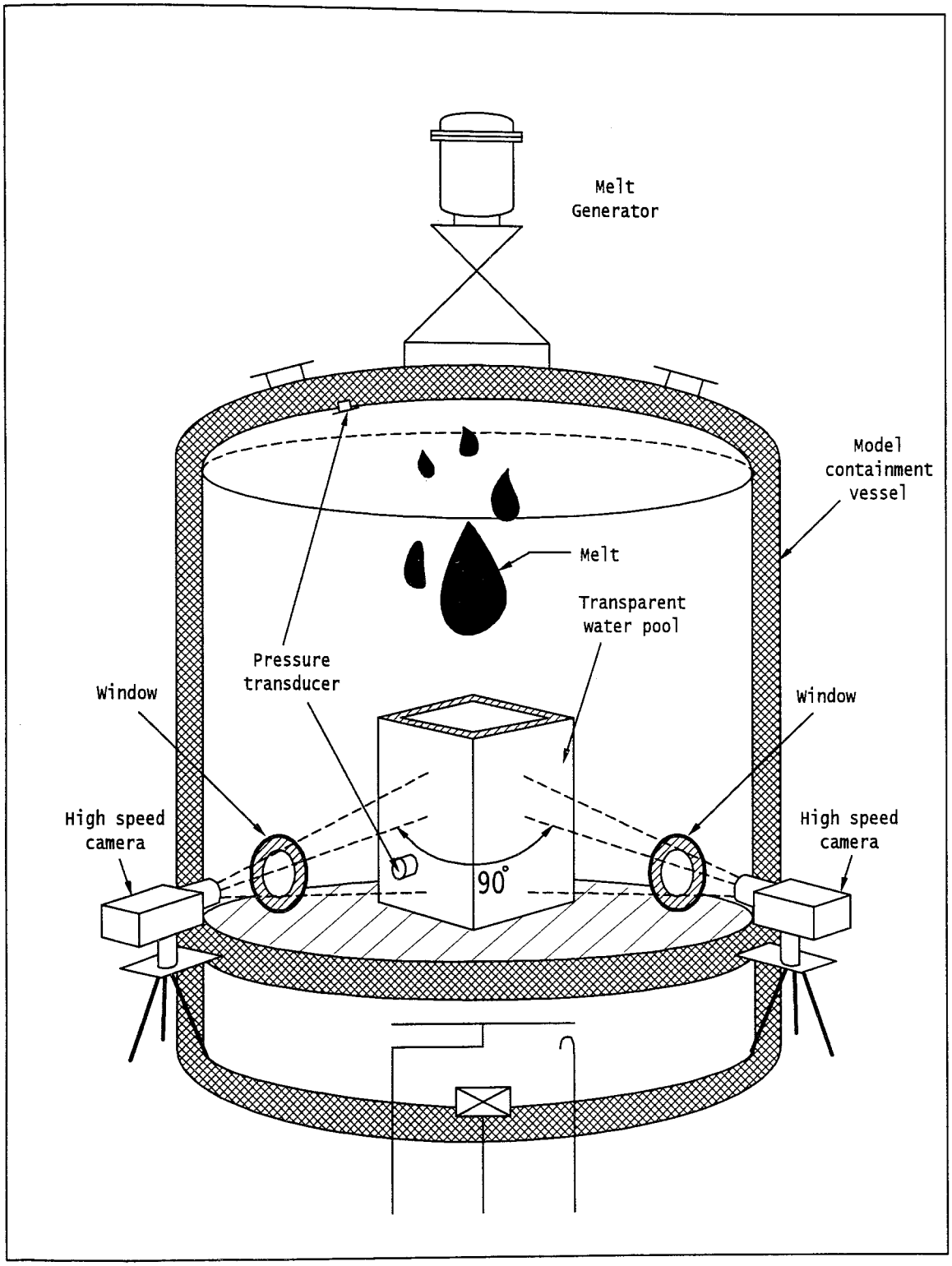

Figure 5.1. Schematic illustration of the ALPHA facility in JAERI, Japan

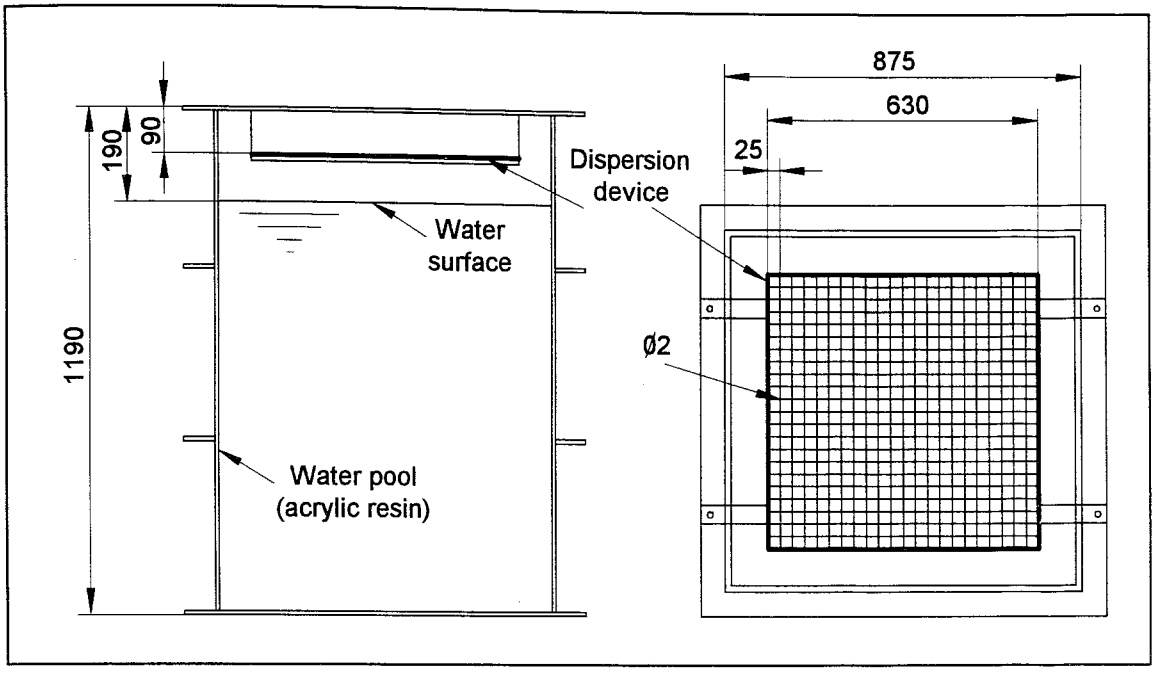

Figure 5.2. Dispersion device and water pool [44]

In some experiments, to force the melt to be dispersed during its free fall, a dispersion device has been used (Figure 5.2.). The dispersion device consists of a 63 X 63 cm grid and a steel frame. To obtain a grid, 2 mm diameter steel wires have been arranged forming 25 X 25 mm squares. Dispersion device is placed 10 cm above the water surface. In one of the experiments the device was 10 cm under the water surface.

The pressure of the gas inside the ALPHA facility and the pressure inside the water pool have been measured by the pressure transducers of strain gage and piezo electric types. The fast temperature change in the atmosphere of the ALPHA facility is measured by four thermocouples having 0.25 mm diameters. There are also two other thermocouples having a diameter of 1.6 mm. During the experiments the fast pressure change is recorded by a high-speed recording system having a frequency of 500 kHz.

Two high-speed cameras having a maximum speed of 5 frames per millisecond have been used to record the experiments. When the cameras start to operate, first their speed increases and then reaches a steady state value. In brief, their speed is not a constant value during an experiment. Therefore, the speed of the cameras has been calculated by the time

marks recorded on the film for the period when the phenomenon was observed. The cameras have been placed such that the angle between the two directions of observation is 90^0 [44].

The distance between the surface of the water and the melt generator is about 3.5m. If the friction applied by the air is neglected, the velocity of the melt at the instant when it enters the water pool is calculated as 8.29m/s. The temperature and the density of the melt are 2700K and 3.62 $^{gr}/_{cm^3}$, respectively [35].

6. EVALUATION OF THE VISUAL DATA AND DISCUSSION

6.1. Steam Explosion Experiments

A series of experimental data obtained in the ALPHA facility of the Severe Accident Research Laboratory of Japan Atomic Energy Research Institute have been evaluated for various conditions [35]. The experimental conditions are seen in Table 6.1. In this section, only the experiments resulted in explosion have been evaluated.

Table 6.1. Experimental conditions for the large-scale steam explosions [35]

Exp. No	Melt Mass (kg)	Pressure (MPa)	Covering Gas	Water Temp. (K)	Water Pool	Water Depth (cm)	Water Mass (kg)
5	20	0.1	Air	300	(L)	100	774
9	20	0.1	N_2	289	(L)	100	777
10	10	0.1	Air	297	(L)	100	774
11*	20	0.1	Air	290	(L)	100	774
16	20	0.1	Air	295	(S)	90	174
17	20	0.1	Air	286	(S)	90	174
19*	20	0.1	Air	281	(M)	90	392
21*	20	0.1	Air	281	(L)	90	697
23	20	0.1	Air	285	(L)	30	358
24	20	0.1	Air	280	(M)	80	318
25	20	0.5	Air	280	(M)	90	416

(L): Large Pool, (M): Medium Pool, (S): Small Pool

In experiment 5 (Figure A. 1.), the first triggering occurred at the upper left hand side of the mixture with respect to camera. Since the melt distribution is three dimensional, it is quite difficult to determine the exact position of the first triggering by means of two dimensional photo when the triggering occurs somewhere inside the three dimensional melt distribution.

* Dispersion device is used.

Most probably, this is the case in experiment 5 (Figure A. 1.). Therefore, the arrows used to show the position of the first triggering point can only give a rough idea about its location.

In experiment 9 (Figure A. 2.), 1.37 milliseconds after the first triggering, expansion (explosion) started. The shock wave couldn't reach the upper right part of the mixture. Therefore, this part of the mixture didn't contribute to the explosion. Although the pressure wave has last reached almost the lowest part of the dispersed melt particles, the expansion started at this location. It has been observed that the pressure wave propagated in any direction randomly and at different speeds. By means of the 10 cm side square mesh drawn on the transparent pool, the movement (displacement) of the shock wave (black region) is determined for the two successive film squares. Because the time between the two successive film squares is known, the propagation velocity is determined by the ratio of the displacement to time.

For experiment 10 (Figure A. 3.), triggering occurred in one of the regions where a high amount of melt particles were present. Just before the triggering a downward acceleration (gravitational acceleration) of the melt has been observed in this region. Since the gravitational force applied on the melt is higher than the buoyancy force, the melt tends to go down. On the other hand, the gravitational force applied on the steam is smaller than the buoyancy force; so, the steam tends to move up. Therefore, higher the concentration of melt in the interaction region, greater the downward acceleration of the melt due to the gravitational force. The author thinks that the combined effects of the gravitational and buoyancy forces cause the steam film around the melt to strip away. That is why the possibility of triggering is high in the regions where the melt is densely located.

Propagation has been accompanied by the expansion. After the first triggering occurred, local expansion started. Although it is well known that the velocity of the propagation wave is greater than that of the expansion, in the direction of expansion the propagation is suppressed due to the high void fraction. The propagation wave couldn't reach the upper right part of the mixture.

For experiment 11 (Figure A. 4.), 0.4 millisecond after the first triggering local expansion started. The propagation of the shock wave continued during 1.21 milliseconds. It has been observed that propagation wave could not penetrate into the region easily where the void fraction (amount of steam) is high. In another words, the molten metal located in the high

void fraction region before the triggering started cannot contribute to the steam explosion. This result is quite understandable, since the propagation wave is transmitted and reinforced by the collapse of the steam films around the neighboring melt particles. If the steam film is too thick or the melt is covered by a high amount of steam, the collapse of steam film is out of question. The expansion caused by the explosion pushed the upper parts of the mixture upward. This region neither triggered nor contributed to the steam explosion. In this experiment, the dispersion device has been placed on the water pool to obtain a finer and more homogeneous melt water mixture in the premixing stage (Figure 5.2.).

For experiment 16 (Figure A. 5.), triggering occurred in the region where the melt is highly accumulated. 0.42 milliseconds after the first triggering the expansion started; however, the pressure wave continued its propagation towards the region where the undisturbed melt particles were present. Just before the triggering has started, a downward acceleration (gravitational settling) in the region where the triggering took place has been observed. According to the author, the same physical mechanism (steam film stripping effect) explained in experiment 10 (Figure A. 3.) is responsible for the triggering.

For experiment 17 (Figure A. 6), triggering occurred at the lowest edge of the dispersed melt region where the fraction of melt was high. When the triggering occurred, the local expansion was so fast that one of the cameras could not detect the propagation. However, the other camera was able to detect the propagation, which took place in 0.6 millisecond. A downward gravitational acceleration in the region where the triggering occurred has been observed just before the triggering started. In this experiment, the propagation wave initiated in the lowest part of the main melt water mixture could not penetrate to the small melt water mixture region which was separated from the main mixture by a mass of water. This is attributed to the fact that the shock wave cannot propagate in the water well. It should be reinforced by the triggering of the other melt particles. If there are no melt particles nearby to be triggered, the shock wave loses its strength.

For experiment 19 (Figure A. 7), the dispersion device has been placed on the 90 cm deep-water pool. Propagation wave passed through the entire melt water mixture region in 0.75 millisecond. 0.75 millisecond after the first triggering the expansion started. In this experiment, by chance an interesting phenomenon has been observed. In all of the other experiments, the beginning of the triggering and subsequent propagation phenomena has been

observed as a small dark region (small dark region characterizes steam). However, in this experiment the triggering initiated as a bright light or a scattering of a cloud of very fine bright particles. For all the experiments, generally, the speed of the camera changes from one frame in 0.3 millisecond to one frame in 0.2 millisecond during the time period from the end of the premixing to the end of the expansion stage. If a phenomenon occurs in less than 0.2 milliseconds, the camera may not detect this phenomenon. Let's assume that this small time interval during the phenomenon occurs is Δt. The probability of this phenomenon to be detected by the camera having a speed of one frame in 0.2 millisecond is $\Delta t / 0.2$. Depending on the magnitude of Δt, this probability can be very small. Although, it is impossible to determine Δt by using a camera having a speed of one frame in 0.2 millisecond, most probably in the experiment 19 (Figure A. 7.), the actual instant when the triggering occurred has been detected by chance. According to the author, the bright image could be the high velocity fragmented melt particles.

For experiment 21 (Figure A. 8.), the dispersion device has been placed under the water level. 0.72 millisecond after the triggering was initiated, the local expansion was observed. Propagation took 0.96 millisecond. As a result of expansion, excessive steam production pushed the untriggered melt particles away. It seemed that another triggering occurred in the middle of the mixing region; and an independent explosion was initiated in the middle part of the melt liquid steam mixture. Void fraction in the upper part of the mixture was high when the triggering initiated; therefore, propagation of the shock wave couldn't reach that region. As a result, the melt particles in the upper part of the mixture couldn't contribute to the explosion.

In experiment 23 (Figure A. 9.), the melt has reached the bottom of the pool in three columns. When the first column has reached the bottom, it simultaneously triggered at the bottom. Local expansion started 0.28 millisecond after the triggering. Almost the same process and the time scales were valid for the other two columns. The columns touched the bottom of the pool one by one with 0.28 millisecond time intervals. The independent explosion of those columns can be attributed to the fact that the pressure wave initiated by one of the columns could not propagate to the other ones, since there were no melt particles to be triggered among the columns to reinforce the propagation of the shock wave; film collapse on the neighboring molten droplet is necessary.

In experiment 23 (Figure A. 9.), shallow water pool is used. For the shallow water pool case, the depth of the water is not enough to slow down the sinking melt until it hits the bottom. According to the author, when the collision velocity is higher, it is more likely that a small amount of water is trapped between the melt and the bottom of the pool. When the trapped water is superheated until its temperature reaches the homogeneous nucleation temperature, it expands in a very short time. This can be the mechanism of the triggering in this experiment.

For experiment 24 (Figure A. 10.), CO_2 was dissolved in the water pool. After the main mass of the melt entered the pool, the triggering initiated simultaneously by another bulk of melt when it touched on the surface of the water where in this region of the water no melt particles entered before. The pressure wave reached the longest distance inside the melt water mixture in 2.1 milliseconds. Because of the lack of melt particles in the region between the first triggering location and the main melt water mixture, the pressure wave could not reach all parts of the mixture easily. 2.4 milliseconds after the triggering, the expansion of the main melt water and steam mixture initiated.

In experiment 25 (Figure A. 11.), a more homogeneous melt water mixture is obtained compared to the other experiments. The triggering occurred at the bottom of the mixture. 0.64 millisecond after the triggering, local expansion started. However, the propagation of the shock wave continued after the expansion. The propagation took about 1.7 milliseconds.

In this section, only the experiments that steam explosion occurred have been examined. Total 23 experiments have been performed. The ambient pressure was 0.1 MPa in 18 experiments. In 12 of those experiments explosion occurred. In another words, 66.6% of the experiments resulted in steam explosion for 0.1 MPa ambient pressure. On the other hand, only in one of the experiments explosion observed among the four experiments done under the condition of elevated ambient pressure. More specifically, ambient pressures were 0.5, 1.0, 1.6 and 1.6 MPa for the four experiments. Only the one done under the condition of 0.5 MPa ambient pressure resulted in steam explosion [35]. This result should not be evaluated as high ambient pressure prevents steam explosion. Actually, the probability of steam explosion decreases with increasing the ambient pressure. According to the model suggested by the

author in the previous sections, local steam production is necessary to accelerate the melt. High ambient pressure reduces the possibility of having explosive local steam production; i.e. reduces the probability of triggering. However, occurrence of triggering itself does not mean that the mixture will explode. As is explained in detail, to obtain a large-scale steam explosion a proper geometry of mixture, void fraction, the right ambient pressure and temperature of both coolant and melt are important.

6.2. Evaluation of the Debris Size Distribution

In this subsection, the debris size distribution will be evaluated for two experiments (Exp.5 and Exp.8) performed in the ALPHA facility of JAERI. Since the increase in the total area of the melt particles after the explosion leads to high heat transfer, it is important to determine the total area increase. In experiment 5 (Figure A. 1.) -explosion occurred, the debris is finer compared to the ones obtained in experiment 8 (explosion didn't occur) (Table 6.2.). Considering that the same amount of melt (20kg) is used for both experiments, the percentage of the total area increase caused by the fine fragmentation can be calculated from the debris size distribution. Please note that because the explosion didn't occur in

Table 6.2. Debris size distribution for exp.5 and 8 [44]

Debris Diameter (μm)	Mass Percentage (%)	
	Experiment 5 (Explosion Occurs)	Experiment 8 (Explosion doesn't occur)
10	1.83	0
20-30-40	10	0.07
50-60-70-80-90	16.67	1.53
100	16	2
200-300-400	22.5	2.8
500-600-700-800-900	16.5	13.6
1000	16.5	80

experiment 8, the melt break-up only took place in the premixing stage due to the hydrodynamic forces caused by the sinking velocity of the melt.

The area enlargement caused by the explosion was compared with the non-explosion case. It has been assumed that the geometry of debris is a sphere. If all the debris's diameters in a certain mass percentage interval are not constant, simply it is assumed that they are equally distributed inside that certain range.

Nomenclature:

M_T = Total mass

V_T = Total volume

ρ = Density of the debris

v_r = The volume of one debris having a radius (r)

x_r = The number of debrises having a radius (r)

m_r = The mass of one debris having a radius (r)

M_r = The total mass of all the debrises having a radius (r)

A_r = The surface area of a debris having a radius (r)

S_r = The total surface area of all the debrises having a radius (r)

S_T = The total surface area of all the debrises

y_r = The total mass percentage of the debrises having a radius (r)

Comparison of the final total surface areas for the explosion and non-explosion cases (Exp.5 and 8):

$$v_r = \frac{4}{3}\pi.r^3 \tag{6.1}$$

$$m_r = \frac{4}{3}\pi.r^3.\rho \tag{6.2}$$

$$x_r.m_r = M_r = M_T.y_r \tag{6.3}$$

$$x_r \cdot \frac{4}{3}\pi . r^3 . \rho = \rho . V_T . y_r \tag{6.4}$$

$$x_r = \frac{3 . y_r}{4 . \pi . r^3} . V_T \tag{6.5}$$

$$A_r = 4 . \pi . r^2 \tag{6.6}$$

$$S_r = x_r . A_r \tag{6.7}$$

$$S_r = \frac{3 . y_r . V_T}{r} \tag{6.8}$$

$$S_T = 3 . V_T \cdot \sum_r \frac{y_r}{r} \tag{6.9}$$

$$\frac{S_{T\,experiment5}}{S_{T\,experiment8}} = \frac{3 . V_T . \left(\sum_r \frac{y_r}{r} \right)_{experiment5}}{3 . V_T . \left(\sum_r \frac{y_r}{r} \right)_{experiment8}} \tag{6.10}$$

From Table 6.2. and Equations (6.1-6.10), it can be calculated that the ratio of the total surface area of all the debrises in experiment 5 (Figure A. 1) to that in experiment 8 is equal to 6.913. In another words, the final total heat transfer area in experiment 5 (Figure A. 1.) (explosion occurred) is only about 7 times greater than that in experiment 8 for the same initial melt mass and volume. If the steam explosion is caused by the increased heat transfer area, the steam production per unit time for a steam explosion experiment should only be about seven times greater than that in the no-explosion case. This explanation is far from the actual situation. Considering that the velocity of the expansion during a steam explosion experiment is 40~70 m/s, there should be a more effective heat transfer mechanism resulting an explosive steam production. The model suggested by the author involves high-speed fragmented particles; therefore, convection will be the main heat transfer mechanism.

7. CONCLUSION

An alternative fragmentation model, which is a combination of hydrodynamic and thermal theories, has been developed for the triggering stage of the steam explosion phenomenon. Concerning the hydrodynamic part of this fragmentation model, pressure distribution over the moving melt has been taken into account instead of boundary layer striping. To calculate the critical velocity of the moving melt, an empirical relation [31] present in the literature has been utilized. Explosive steam production as a result of steam film collapse, and, subsequent steam penetration into the melt constitute the thermal part of this alternative fragmentation model. Under the conditions of the large-scale steam explosion experiments previously done in the ALPHA facility of Japan Atomic energy Research Institute [35], the model equations have been solved; and, the heat transfer coefficient (h) is found as $25.182x10^{6} Wm^{-2}K^{-1}$ at the instant when the fragmentation just starts. Note that the heat transfer by means of radiation is also included in the convection term. The heat transfer coefficient has been compared with the values present in the literature. The calculated heat transfer coefficient value is at the same order of magnitude and slightly bigger than that is present in the literature due to the reasons previously explained.

The critical relative velocity necessary to initiate the fragmentation process is calculated as $0.775\ ms^{-1}$. The author would like to put an emphasis on the fact that the motion of the melt is a random vibration, such that a macro scale displacement of the molten droplet cannot be observed at the triggering stage. Based on the heat transfer coefficient calculated by means of solving the model equations, steam production per unit time is high enough to obtain a shock wave, which is one of the necessary conditions to have a large-scale steam explosion. In other words, at the triggering stage, steam water interface moves faster than the speed of sound in the water for the given experimental conditions. Then the shock wave (propagation wave) is created. For the calculation of heat transfer coefficient, an uncertainty analysis has been done. Depending on the several parameters used in the model equations, an uncertainty range for the heat transfer coefficient was found ($25.182\text{-}28.2\text{x}10^{6} Wm^{-2}K^{-1}$). It was indicated that even the smallest value of the heat transfer coefficient ($25.182\text{x}10^{6} Wm^{-2}K^{-1}$) in the uncertainty range is high enough to initiate a shock wave.

The speed of the camera is not high enough to detect the triggering of only one melt droplet, which takes place much less than one millisecond. Therefore, there is no strong visual experimental evidence to support this theory. However, in one of the large-scale steam explosion experiments (exp. 19) previously done in the ALPHA facility of JAERI, a bright light which looks like scattering of a cloud of very fine bright particles has been detected in the interaction region where the triggering initiated. The author thinks that the bright light may characterize the vibrating fragmented molten particles mentioned in the suggested model. Since triggering occurs in a very short time, it may have been detected only in one of the experiments by chance.

According to the model introduced in this Ph.D. thesis, an explosive local steam production on the melt droplet where the film collapse occurs is necessary to get a propulsive force. If the ambient pressure is increased, it will be more difficult to have an explosive local steam production or violent boiling, which leads to the acceleration of the melt droplet. As a result, high ambient pressure will reduce the possibility of triggering. This result is in good agreement with the large-scale steam explosion experiments previously performed in the ALPHA facility of JAERI (there is only one exceptional experiment) [35]. However, this result should not give a misleading impression that high ambient pressure prevents steam explosions! The correct conclusion is that a stronger trigger pulse (probably forced triggering) is necessary to initiate the propagation for the high ambient pressures.

Referring to the visual data of the ALPHA experiments [35], it has been observed that the propagation of the shock wave is very difficult or impossible in the regions where the void fraction rate is high. According to the experimental data the shock wave cannot propagate well in the regions where the distances among the melt particles are long. Generally, all of the melt particles have not contributed to the explosion; instead, some of them have been pushed away by the large-scale expansion (steam production). In one of the experiments (exp.23) done in the shallow water pool, the collision of the three melt columns with the bottom of the pool triggered the subsequent explosions one by one. Of course, sinking velocity of the melt at the instant of collision with the bottom of a shallow pool is higher compared to the case of a deeper pool. According to the author, for the higher sinking velocities, since the coolant beneath the melt has a certain inertia, it is more likely that a small amount of water can be trapped between the melt and the bottom of the pool. Superheating of the trapped water until the homogeneous nucleation temperature, and subsequent expansion should be the reason of

triggering in the locations where the collisions occurred.

It has been observed that the sinking velocity of the mixture is not the same everywhere in the interaction region. Generally, triggering occurs in the region where a local acceleration (gravitational acceleration at the regions where the melt is densely located) is observed. This is attributed to the fact that the combined effect of the drag force increased by the acceleration and the buoyancy force due to the density difference between the steam film and the water causes the steam film to collapse locally or to strip away. This mechanism can initiate triggering by causing the water to contact directly with the melt.

Using the debris size distribution data of the ALPHA experiments [44], the ratio of the total final surface area of all the fragmented particles for an experiment in which explosion occurred to that of a no explosion experiment has been calculated. This value is about seven. In other words, the final heat transfer surface area of a large-scale steam explosion experiment is about seven times greater than that of a no explosion experiment for the same amount of melt and water mass. Regarding to the qualitative examination of the large-scale steam explosion experiments, the author observed that steam production per unit time at the expansion stage of a steam explosion is thousands of times greater than the steam production per unit time for a no explosion experiment. The author concludes that only seven times enlargement of the heat transfer area cannot explain this huge amount of destructive steam production per unit time. Therefore, an alternative approach that takes into consideration the relative velocities, as in the case of the suggested theory, should be involved.

APPENDIX: VISUAL DATA OF THE LARGE-SCALE STEAM EXPLOSION EXPERIMENTS

In the following pages of this section, visual data of the large-scale steam explosion experiments have been presented [35]. The researchers of the Severe Accident Research Laboratory (SARL) of Japan Atomic Energy Research Institute (JAERI) previously have done the large-scale steam explosion experiments. The experimental data accumulated since 1991 have been obtained by using the ALPHA (Assessment of Loads and Performance of containment in a Hypothetical Accident) facility of Japan Atomic Energy Research Institute. The author also contributed to the digitalization of the visual data of the large-scale steam explosion experiments during his stay in Japan Atomic Energy Research Institute.

On the following pages, only the experiments in which explosion occurred have been presented. Complete visual data can be seen in reference [35]. The vertical and horizontal arrows indicate the location of triggering in the interaction region. Dark color regions represent steam. On the visual data, triggering can be observed as a small dark spot. After that, the dark spot becomes larger spreading the interaction region. The expanding dark region characterizes the escalation or pressure wave.

T=0. 00 millisecond

T=0. 80 millisecond

T=0. 27 millisecond

T=1. 07 millisecond

T=0. 54 millisecond

T=1. 34 millisecond

Figure A. 1. Experiment 5 con't

T=1. 61 millisecond

T=2. 41 millisecond

T=1. 88 millisecond

T=2. 68 millisecond

T=2. 14 millisecond

T=2. 95 millisecond

Figure A. 1. (Continued) con't

T=3. 22 millisecond

T=4. 02 millisecond

T=3. 48 millisecond

T=4. 29 millisecond

T=3. 75 millisecond

T=4. 56 millisecond

Figure A. 1. (Continued)

con't

T=4. 82 millisecond

T=5. 63 millisecond

T=5. 09 millisecond

T=5. 90 millisecond

T=5. 36 millisecond

T=6. 16 millisecond

Figure A. 1. (Continued)

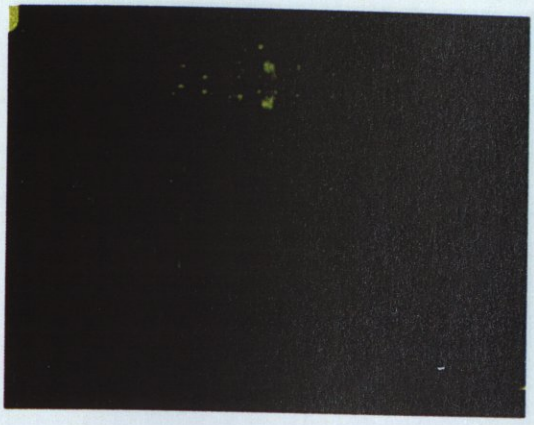

T=-214.32 millisecond

T=-100.32 millisecond

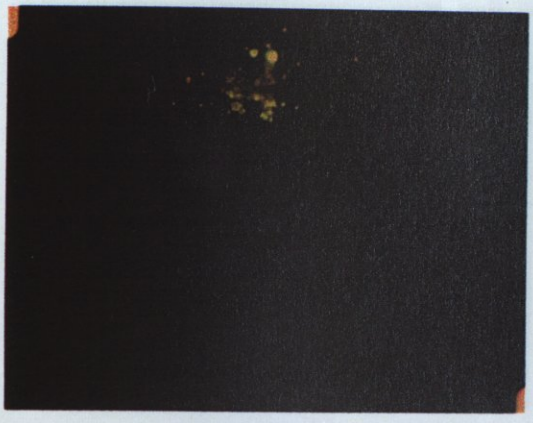

T=-191.52 millisecond

T=-54.72 millisecond

T=-168.72 millisecond

T=0.00 millisecond

Figure A. 2. Experiment 9

con't

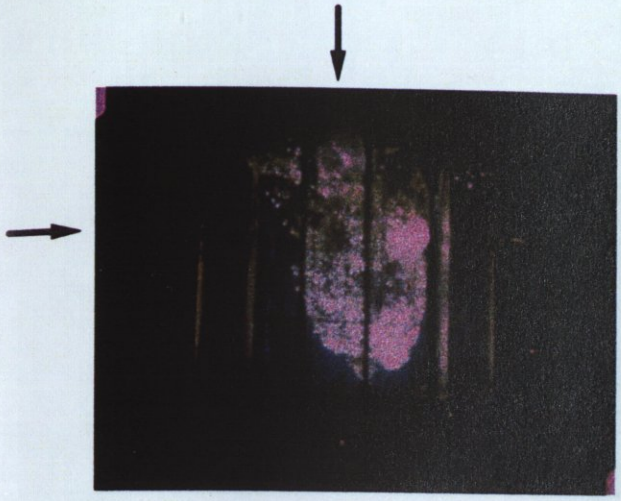

T=0. 23 millisecond

T=0. 91 millisecond

T=0. 46 millisecond

T=1. 14 millisecond

T=0. 68 millisecond

T=1. 37 millisecond

Figure A. 2. (Continued) con't

T=1. 60 millisecond

T=2. 28 millisecond

T=1. 82 millisecond

T=2. 51 millisecond

T=2. 05 millisecond

T=2. 74 millisecond

Figure A. 2. (Continued) con't

T=2. 96 millisecond

T=3. 19 millisecond

Figure A. 2. (Continued)

T=-220. 90 millisecond

T=-103. 40 millisecond

T=-197. 40 millisecond

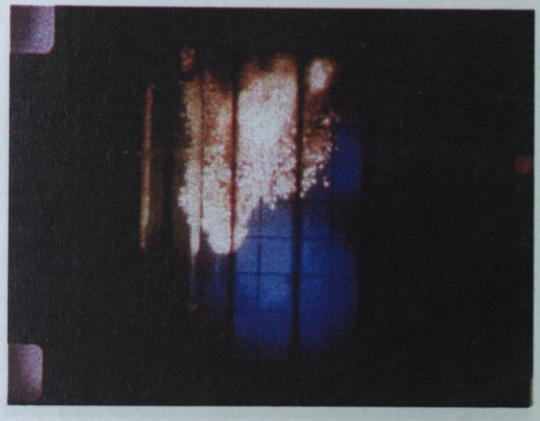

T=-56. 40 millisecond

T=-173. 90 millisecond

T=0. 00 millisecond

Figure A. 3. Experiment 10 con't

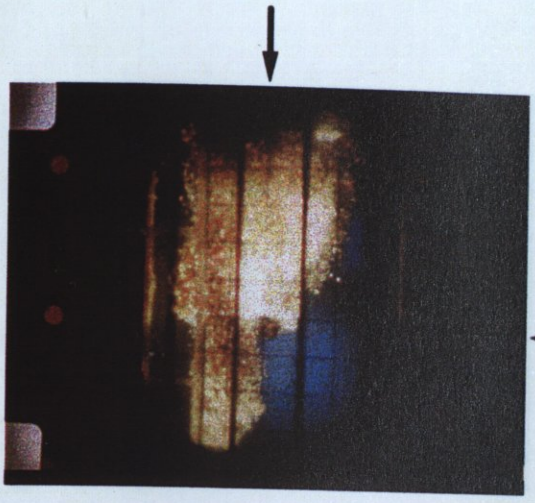

T=0. 24 millisecond

T=0. 94 millisecond

T=0. 47 millisecond

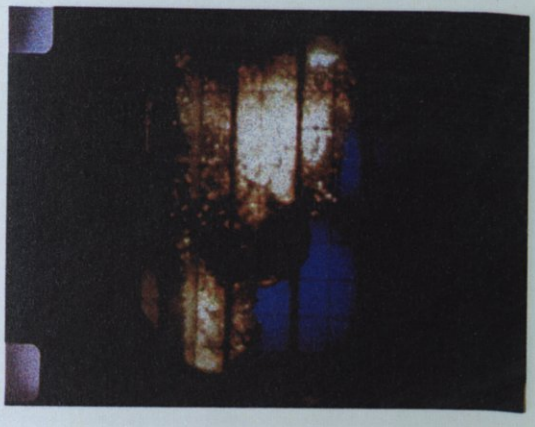

T=1. 18 millisecond

T=0. 71 millisecond

T=1. 41 millisecond

Figure A. 3. (Continued)

con't

T=1. 65 millisecond

T=2. 36 millisecond

T=1. 88 millisecond

T=2. 60 millisecond

T=2. 12 millisecond

T=2. 84 millisecond

Figure A. 3. (Continued)

con't

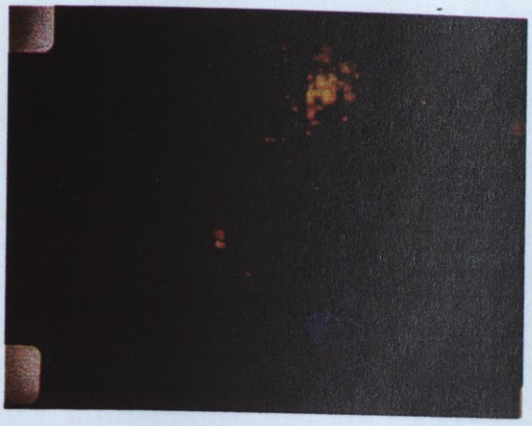

T=3. 08 millisecond

T=3. 80 millisecond

T=3. 32 millisecond

T=3. 56 millisecond

Figure A. 3. (Continued)

T=0. 00 millisecond

T=0. 60 millisecond

T=0. 20 millisecond

T=0. 80 millisecond

T=0. 40 millisecond

T=1. 00 millisecond

Figure A. 4. Experiment 11 con't

T=1. 21 millisecond

T=1. 82 millisecond

T=1. 41 millisecond

T=2. 02 millisecond

T=1. 62 millisecond

T=2. 22 millisecond

Figure A. 4. (Continued)

con't

T=2. 42 millisecond

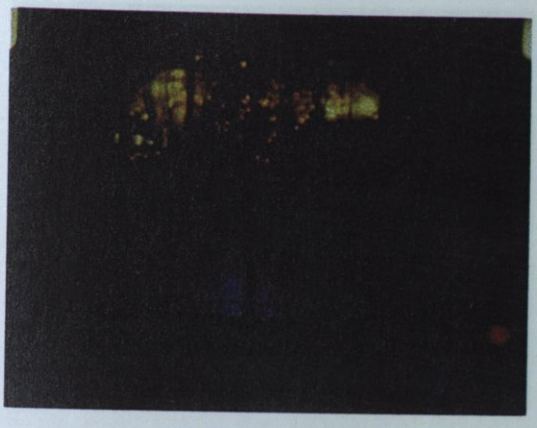

T=3. 03 millisecond

T=2. 63 millisecond

T=3. 23 millisecond

T=2. 83 millisecond

T=3. 43 millisecond

Figure A. 4. (Continued)

T=-294.35 millisecond

T=-192.85 millisecond

T=-274.05 millisecond

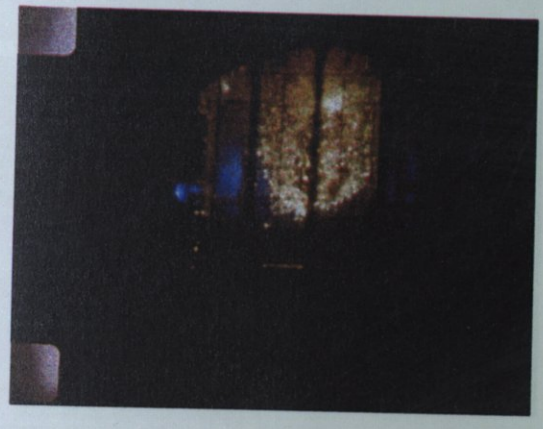

T=-91.35 millisecond

T=-253.75 millisecond

T=-10.15 millisecond

Figure A. 5. Experiment 16

con't

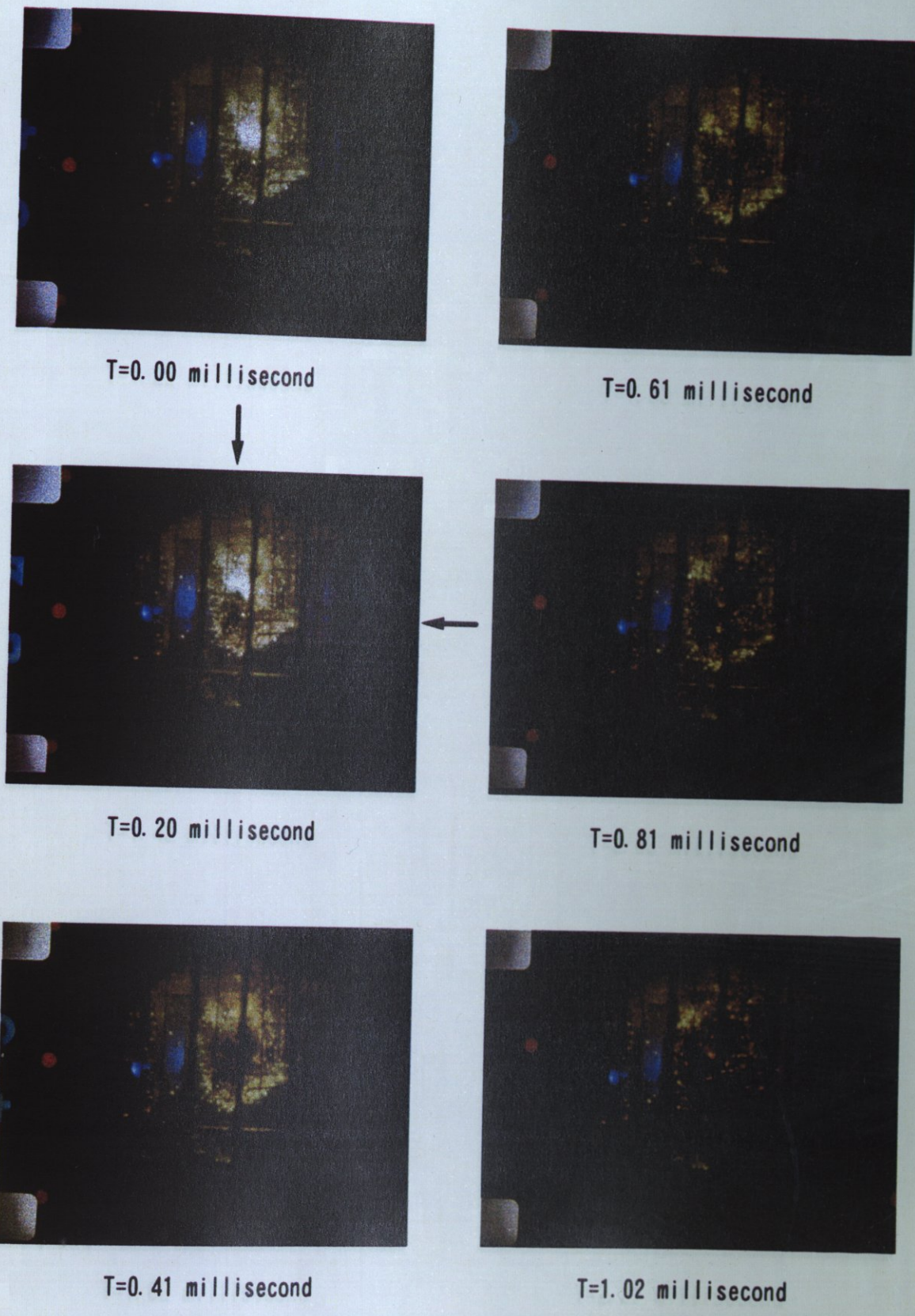

Figure A. 5. (Continued)

con't

T=1. 22 millisecond

T=1. 83 millisecond

T=1. 42 millisecond

T=2. 03 millisecond

T=1. 62 millisecond

T=2. 23 millisecond

Figure A. 5. (Continued)

con't

T=2. 44 millisecond

T=3. 05 millisecond

T=2. 64 millisecond

T=3. 25 millisecond

T=2. 84 millisecond

T=3. 45 millisecond

Figure A. 5. (Continued)

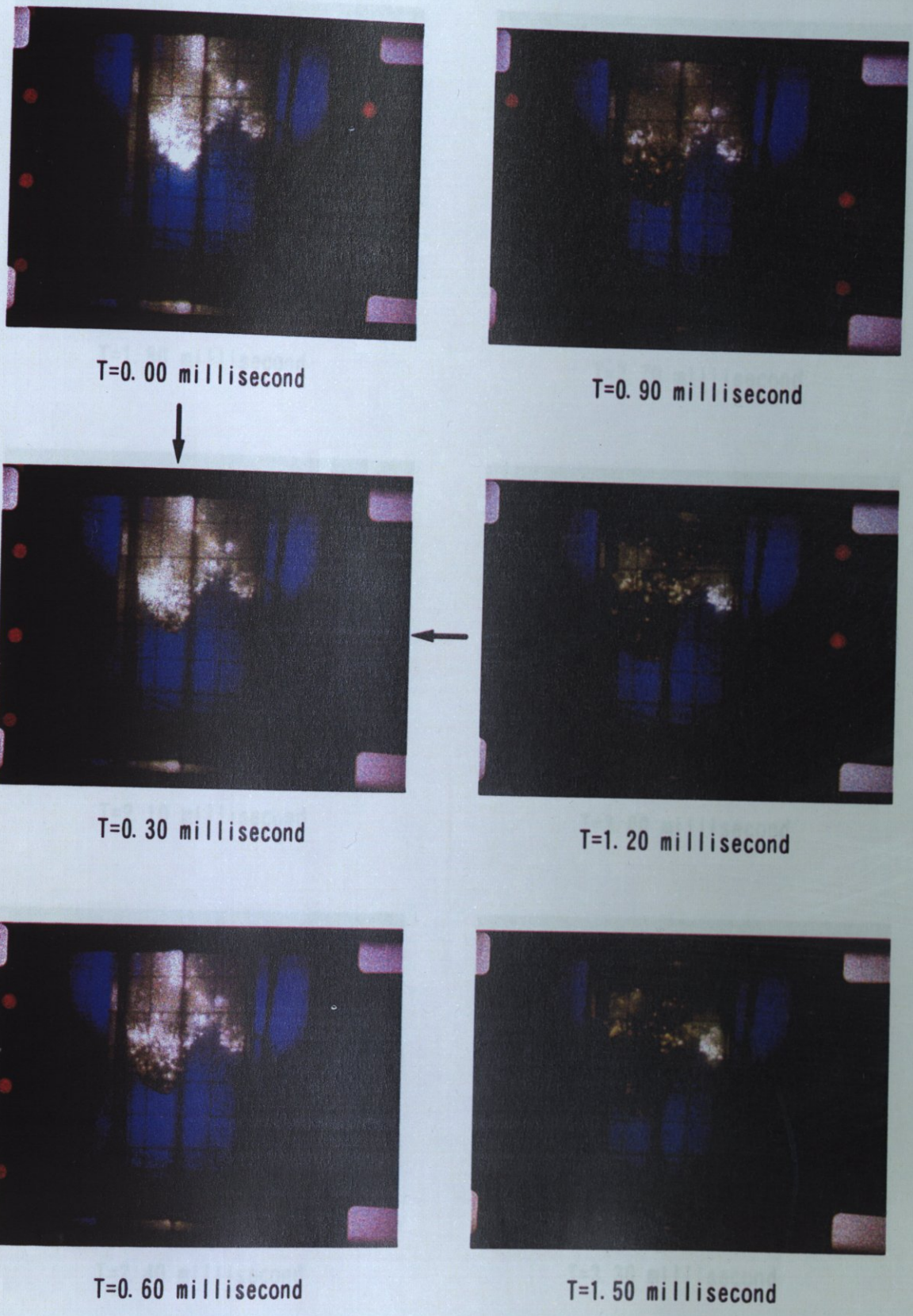

Figure A. 6. Experiment 17 con't

T=1. 80 millisecond

T=2. 70 millisecond

T=2. 10 millisecond

T=3. 00 millisecond

T=2. 40 millisecond

T=3. 30 millisecond

Figure A. 6. (Continued)

con't

T=3. 60 millisecond

T=4. 50 millisecond

T=3. 90 millisecond

T=4. 80 millisecond

T=4. 20 millisecond

Figure A. 6. (Continued)

T=0. 00 millisecond

T=0. 75 millisecond

T=0. 25 millisecond

T=1. 00 millisecond

T=0. 50 millisecond

T=1. 26 millisecond

Figure A. 7. Experiment 19

con't

T=1. 51 millisecond

T=2. 26 millisecond

T=1. 76 millisecond

T=2. 51 millisecond

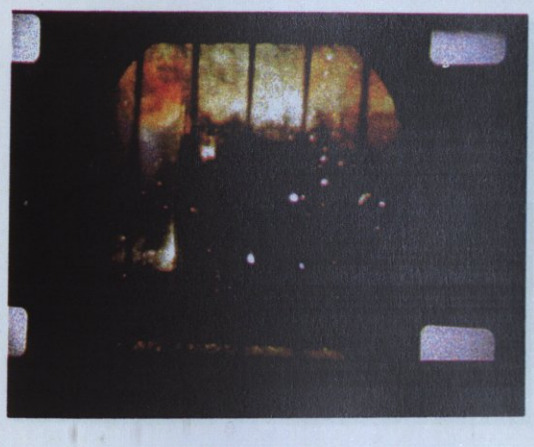

T=2. 01 millisecond

T=2. 76 millisecond

Figure A. 7. (Continued)

con't

T=3. 01 millisecond

T=3. 77 millisecond

T=3. 26 millisecond

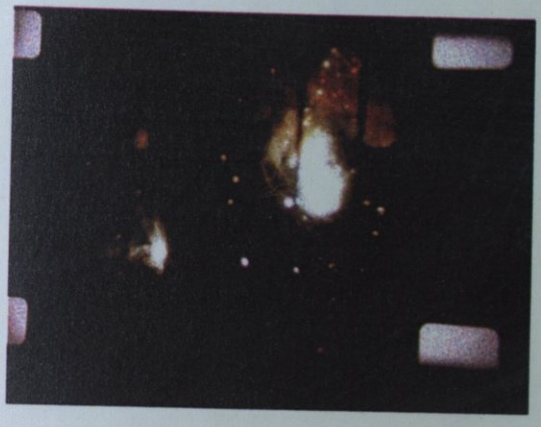

T=4. 02 millisecond

T=3. 51 millisecond

T=4. 27 millisecond

Figure A. 7. (Continued)

con't

T=4. 52 millisecond

T=5. 27 millisecond

T=4. 77 millisecond

T=5. 02 millisecond

Figure A. 7. (Continued)

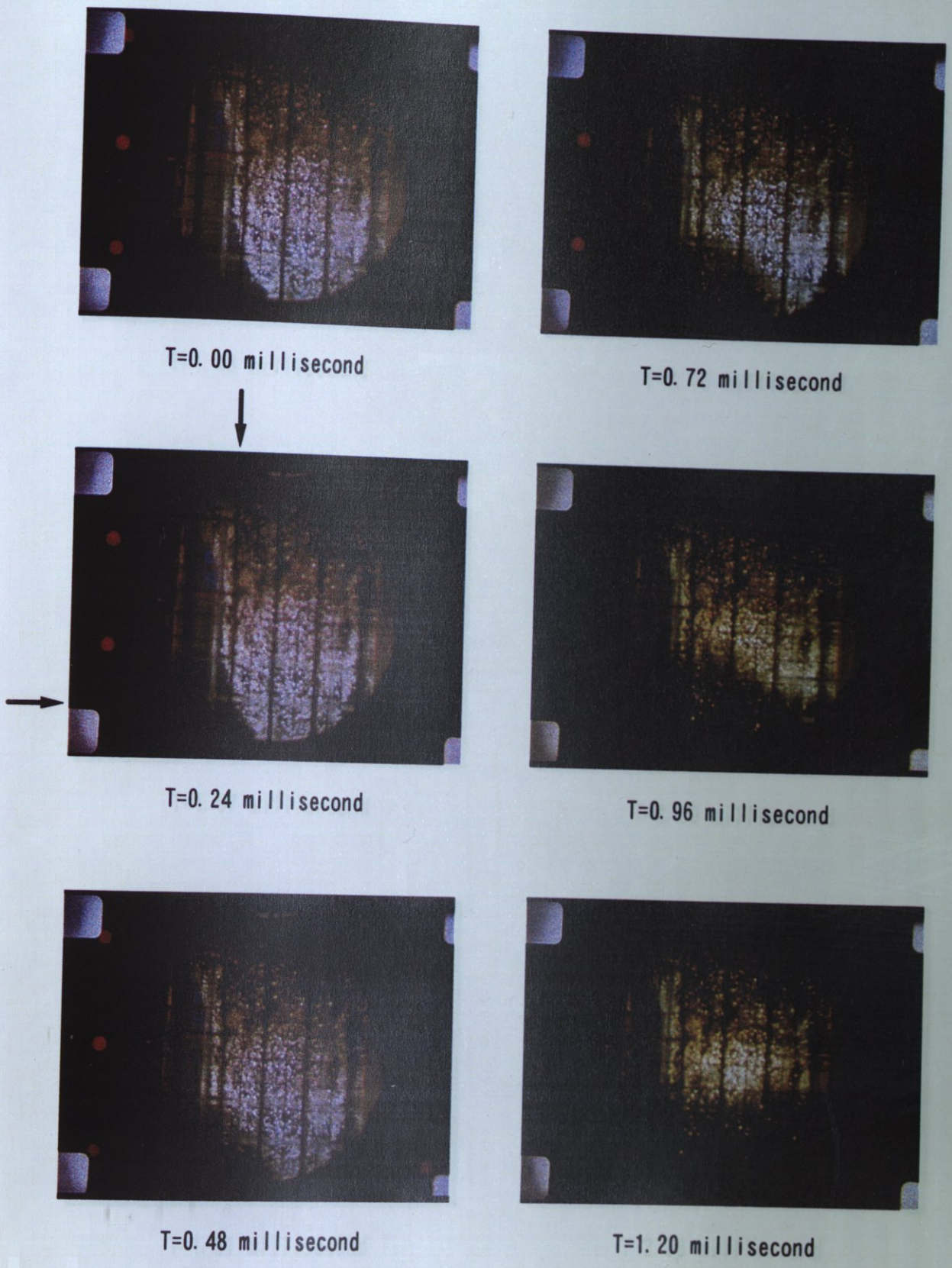

Figure A. 8. Experiment 21

con't

T=1. 43 millisecond

T=2. 15 millisecond

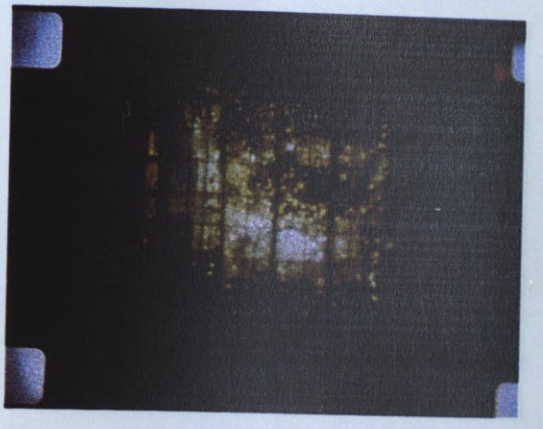

T=1. 67 millisecond

T=2. 39 millisecond

T=1. 91 millisecond

T=2. 63 millisecond

Figure A. 8. (Continued)

con't

T=2. 87 millisecond

T=3. 59 millisecond

T=3. 11 millisecond

T=3. 82 millisecond

T=3. 35 millisecond

T=4. 06 millisecond

Figure A. 8. (Continued)

T=-50. 96 millisecond

T=-17. 36 millisecond

T=-50. 40 millisecond

T=-8. 96 millisecond

T=-28. 56 millisecond

T=-3. 36 millisecond

Figure A. 9. Experiment 23 con't

T=-0. 56 millisecond

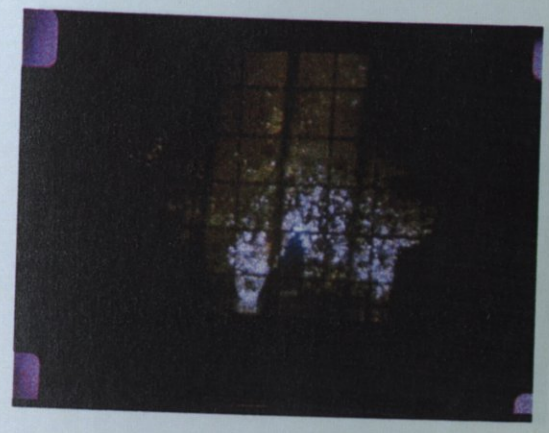

T=0. 56 millisecond

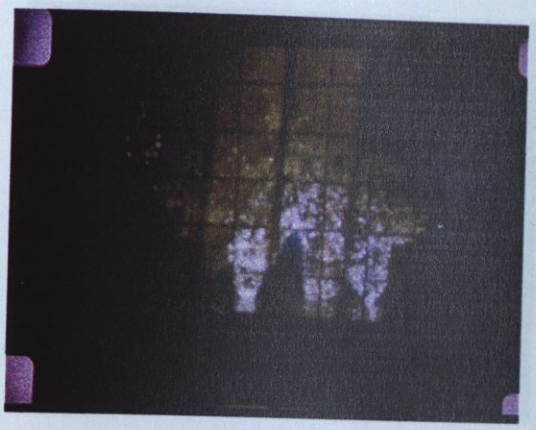

T=0. 00 millisecond

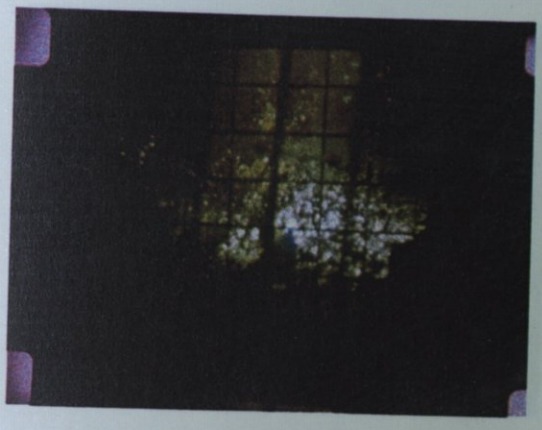

T=0. 84 millisecond

T=0. 28 millisecond

T=1. 12 millisecond

Figure A. 9. (Continued)

con't

T=1. 40 millisecond

T=2. 24 millisecond

T=1. 68 millisecond

T=2. 52 millisecond

T=1. 96 millisecond

T=2. 80 millisecond

Figure A. 9. (Continued)

con't

T=3. 08 millisecond

T=3. 92 millisecond

T=3. 36 millisecond

T=4. 20 millisecond

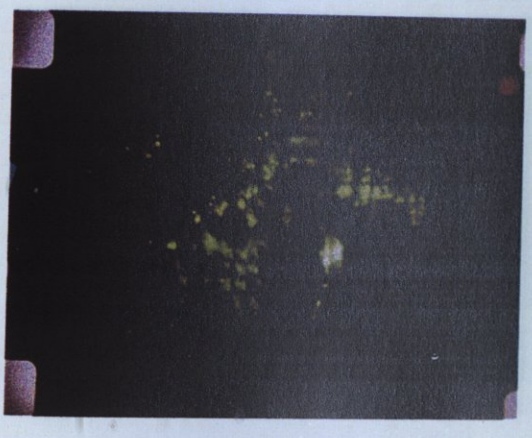

T=3. 64 millisecond

T=4. 48 millisecond

Figure A. 9. (Continued)

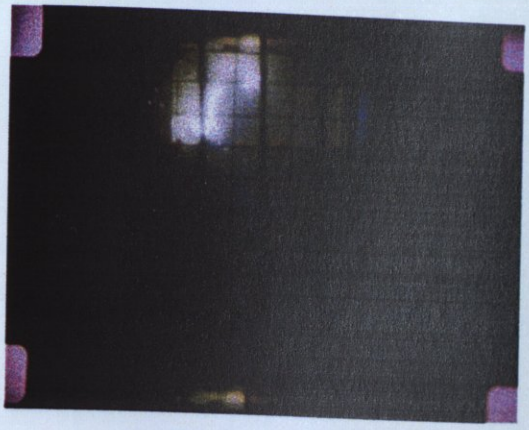

T=-23.63 millisecond

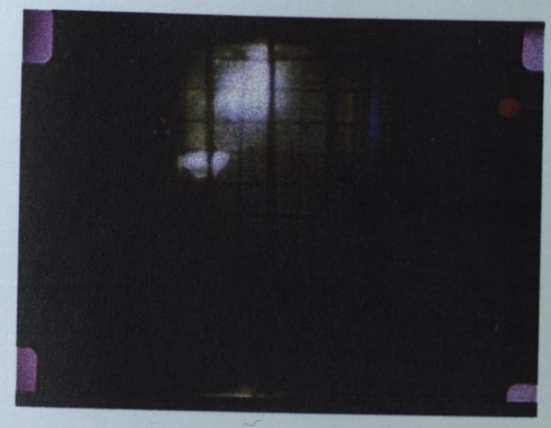

T=-14.54 millisecond

T=-20.60 millisecond

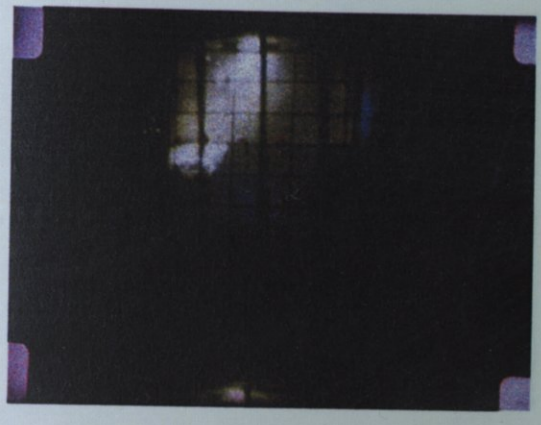

T=-11.51 millisecond

T=-17.57 millisecond

T=-8.48 millisecond

Figure A. 10. Experiment 24 con't

T=-5. 45 millisecond

T=-0. 91 millisecond

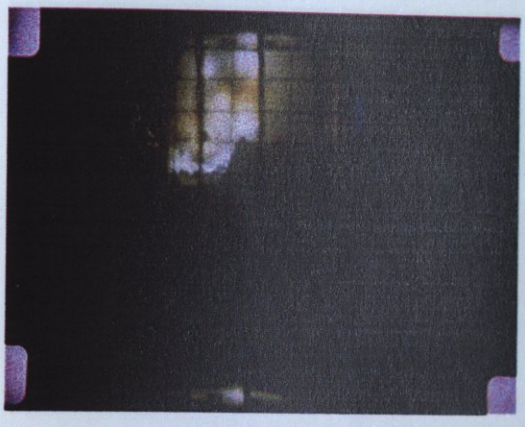

T=-3. 94 millisecond

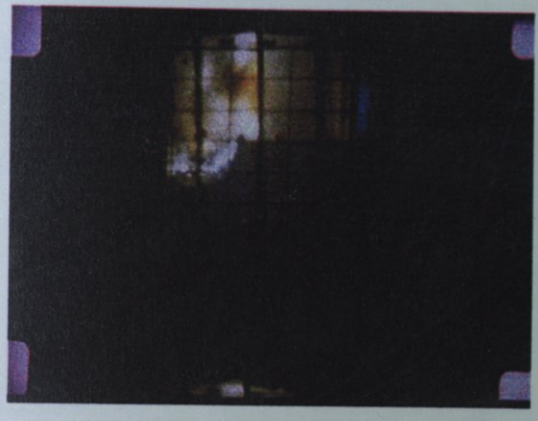

T=0. 00 millisecond

T=-2. 42 millisecond

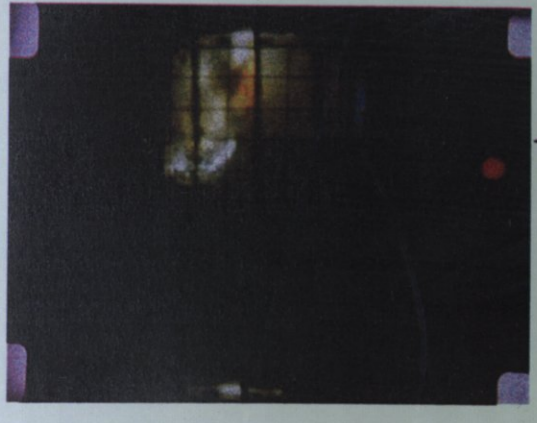

T=0. 30 millisecond

Figure A. 10. (Continued)

con't

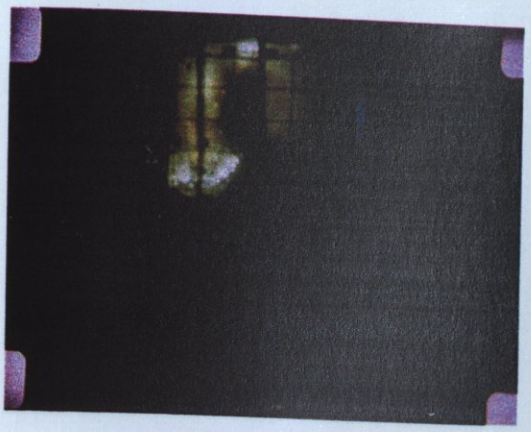

T=0. 61 millisecond

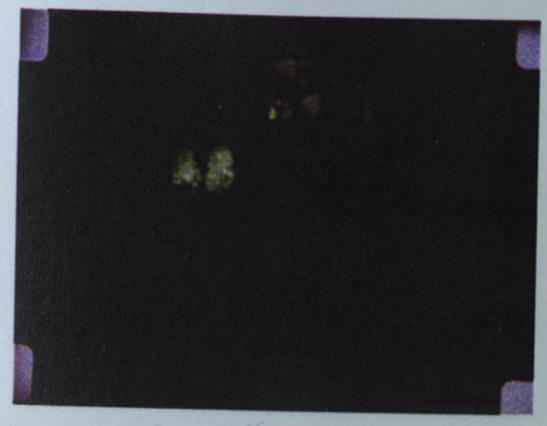

T=1. 52 millisecond

T=0. 91 millisecond

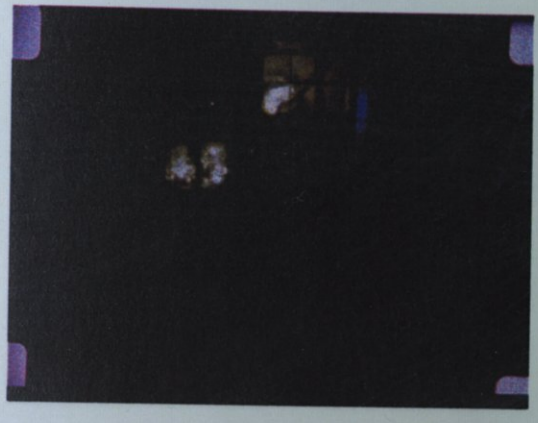

T=1. 82 millisecond

T=1. 21 millisecond

T=2. 12 millisecond

Figure A. 10. (Continued)

con't

T=2. 42 millisecond

T=3. 33 millisecond

T=2. 73 millisecond

T=3. 64 millisecond

T=3. 03 millisecond

T=3. 94 millisecond

Figure A. 10. (Continued) con't

T=4. 24 millisecond

T=5. 15 millisecond

T=4. 55 millisecond

T=5. 45 millisecond

T=4. 85 millisecond

T=5. 76 millisecond

Figure A. 10. (Continued)

T=0. 00 millisecond

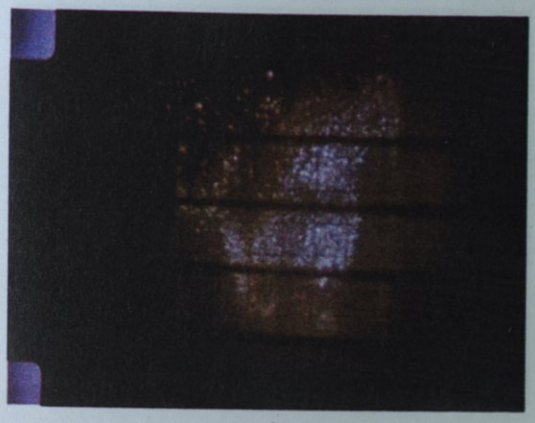

T=0. 64 millisecond

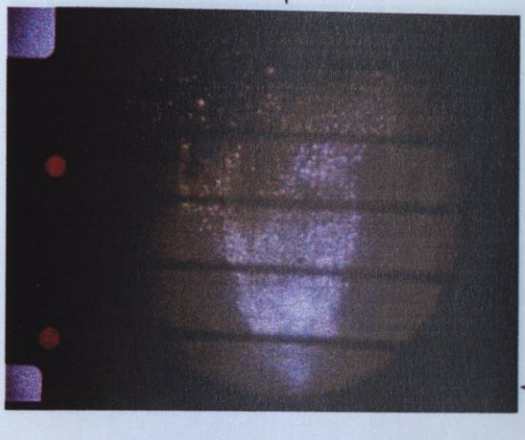

T=0. 21 millisecond

T=0. 85 millisecond

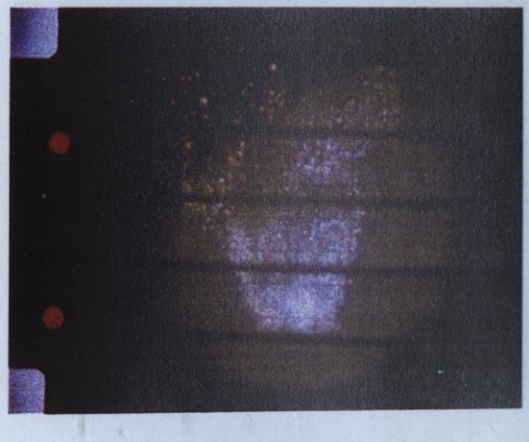

T=0. 42 millisecond

T=1. 06 millisecond

Figure A. 11. Experiment 25 con't

T=1. 27 millisecond

T=1. 91 millisecond

T=1. 48 millisecond

T=2. 12 millisecond

T=1. 70 millisecond

T=2. 33 millisecond

Figure A. 11. (Continued) con't

T=2. 54 millisecond

T=3. 18 millisecond

T=2. 76 millisecond

T=3. 39 millisecond

T=2. 97 millisecond

T=3. 60 millisecond

Figure A. 11. (Continued) con't

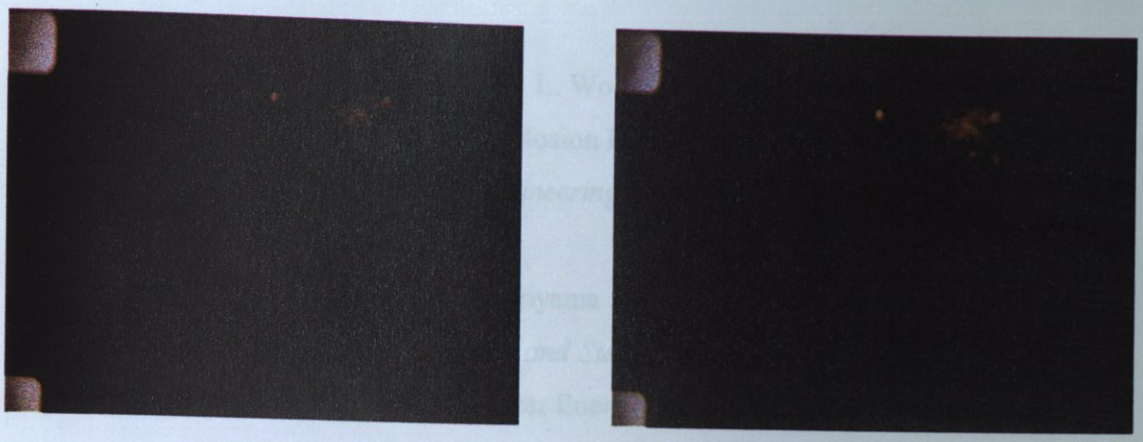

Figure A. 11. (Continued)

REFERENCES

1. Corradini, M. L., D. V. Swenson, R. L. Woodfin and L. E. Voelker, "An Analysis of Containment Failure by a Steam Explosion Following a Postulated Core Meltdown in a Light Water Reactor", *Nuclear Engineering and Design*, Vol. 66, pp. 287-298, 1981.

2. Yamano, N., Y. Maruyama, K. Moriyama and J. Sugimoto, *Technical Note on Ex-vessel Core Melt Debris Coolability and Steam Explosions*, Committee on the Safety of Nuclear Installations OECD Nuclear Energy Agent, December 1996.

3. Matsumura, K., H. Nariai and M. Sakurai, "Thermal Interaction Zone and Self-Triggering Mechanism of Tin-Water Systems", *A Multidisciplinary International Seminar on Intense Multiphase Interactions*, Santa Barbara, June 9-13, 1995.

4. Park, H. S., N. Yamano, Y. Maruyama, K. Moriyama, T. Kudo and J. Sugimoto, *Reviews of Experimental Studies on Various Geometrical Contact Modes in Vapor Explosions*, JAERI-Review 96-018, Japan Atomic Energy Research Institute, 1996.

5. Park, H. S., N. Yamano, Y. Maruyama, K. Moriyama, T. Kudo, Y. Yang and J. Sugimoto, *Design and First Integral Test of Muse Facility in Alpha Program*, JAERI Tech 98-007, Japan Atomic Energy Research Institute, 1998.

6. Long, G., "Explosions of Molten Aluminum in Water-Cause and Prevention", *Metal Progress*, Vol. 71, pp.107-112, 1957.

7. Yamano, N., K. Moriyama, Y. Maruyama, H. S. Park, Y. Yang and J. Sugimoto, *Study on Premixing Phase of Steam Explosion at JAERI*, JAERI-Conf. 97-001, Severe Accident Research Laboratory, Japan Atomic Energy Research Institute, pp.447-467, 1997.

8. Fletcher, D. F. and A. Thyagaraja, "The Chymes Coarse Mixing Model", *Progress in Nuclear Energy*, Vol.26, No.1, pp. 31-61, 1991.

9. Theofanous, T. G., " The in-Vessel Retention as a Severe Accident Management Strategy", *8th International Topical Meeting on Nuclear Reactor Thermal-Hydraulics Proceedings*, Vol.1, Kyoto, Japan, September30- October4, 1997.

10. Moriyama, K., N. Yamano, Y. Maruyama, T. Kudo and J. Sugimoto, " Study of Premixing Phase of Steam Explosion with Jasmine Code in Alpha Program", *Proceedings of the ASME-JSME, 4th International Conference on Nuclear Engineering*, Book No.1389A2-1996, pp.903-915, 1996.

11. Fletcher, D. F., "A Review of the Available Information on the Triggering Stage of a Steam Explosion", *Nuclear Safety*, Vol.35, No.1, pp.36-57, 1994.

12. Matsumura, K., H. Nariai, Y. Egashira and M. Ochimizu, "Experimental Study on the Base Triggered Spontaneous Vapor Explosions for Molten Tin-Water System", *The International Seminar on Vapor Explosions and Explosive Eruptions*, Sendai, Japan, pp. 27-32, May 22-25, 1997.

13. Board, S. J., R. W. Hall and R. S. Hall, "Detonation of Fuel Coolant Explosions", *Nature*, Vol.254, pp.319-321, 1975.

14. Hall, R. W. and S. J. Board, "The Propagation of Large Scale Thermal Explosions", *Int. Journal of Heat and Mass Transfer*, Vol.22, pp.1083-1093, 1979.

15. Fletcher, D. F. and T. G. Theofanous, " Heat Transfer and Fluid Dynamic Aspects of Explosive Melt-Water Interactions", *Advances in Heat Transfer*, Vol.29, pp.129-213, 1997.

16. Fletcher, D. F. and R. P. Anderson, "A Review of Pressure-Induced Propagation Models of the Vapor Explosion Process", *Progress in Nuclear Energy*, Vol.23, No.2, pp.137-179, 1990.

17. Groenveld, P., "Explosive vapor Formation", *Journal of Heat Transfer, Transactions of the ASME*, pp.236-238, 1972.

18. Matsumura, K. and H. Nariai, "Self-Triggering Mechanism of Vapor Explosions for a Molten Tin and Water System", *Journal of Nuclear Science and Technology*, Vol.33, No.4, pp.298-306, 1996.

19. Bankoff, S. G. and J. W. Yang, "On the Physics of Escalation and Propagation of Vapor Explosions", *Proceedings of the International Seminar on the Physics of Vapor Explosions*, Japan, pp.139-148., October 25-29, 1993.

20. Tsuruta, T., T. Hatabu, M. Tsuboi, K. Harada and T. Masuoka, "Experimental Study on Self-Triggering Interaction between Melt and Water", *The International Seminar on Vapor Explosions and Explosive Eruptions*, Japan, pp. 33-39, May 22-25, 1997.

21. Epstein, M., "A New Look at the Cause of Thermal Fragmentation", *Transactions of the American Nuclear Society*, Vol.19, pp.249, 1974.

22. Board, S. J., A. J. Clare, R. B. Bussey, R. S. Hall and D. H. Poole, "An Experimental Study of Energy Transfer Processes Relevant to Thermal Explosions", *Int. Journal of Heat and Mass Transfer*, Vol.14, pp.1631-1641, 1971.

23. Buchanan, D. J., "A Model for Fuel-Coolant Interactions", *Journal of Phys. D., App. Phys.*, Vol.7, pp.1441-1457, 1974.

24. Kim, B. and M. L. Corradini, "Modeling of Small-Scale Single Droplet Fuel/Coolant Interactions", *Nuclear Science and Engineering*, Vol. 98, pp.16-28, 1998.

25. Simpkins, P. G. and E. L. Bales, "Water-Drop Response to Sudden Accelerations", *Journal of Fluid Mechanics*, Vol.55, Part 4, pp. 629-639, 1972.

26. Harper, E. Y., G. W. Grube and I. D. Chang, "On the Breakup of Accelerating Liquid Drops", *Journal of Fluid Mechanics*, Vol.52, Part 3, pp.565-591, 1972.

27. Ranger, A. A. and J. A. Nicholls, "Aerodynamic Shattering of Liquid Drops", *AIAA Journal*, Vol.7, No.2, pp 285-290, 1969.

28. Waldman, G. D. and W. G. Reinecke, "Raindrop Breakup in the Shock Layer of a High-Speed Vehicle", *AIAA Journal*, Vol.10, No.9, pp.1200-1204, 1972.

29. Ciccarelli, G. and D. Frost, "Fragmentation Mechanisms Based on Single Drop Steam Explosion Experiments Using Flash X-Ray Radiography", *Nuclear Engineering and Design*, Vol.146, pp.109-132, 1994.

30. Dowling, M. F., B. M. Ip and S. I. Abdel-Khalik, "Suppression of Vapor Explosions by Dilute Aqueous Polymer Solutions", *Nuclear Science and Engineering*, Vol.113, pp.300-313, 1993.

31. Brodkey, R. S., *The Phenomena of Fluid Motions*, Addision-Wesley, Reading, Mass., 1969.

32. GeLFand, B. E., S. A. Gubin, S. M. Kogarko and S. P. Komar, "Singularities of the Breakup of Viscous Liquid Droplets in Shock Waves", *Journal of Engineering Physics*, Vol.25, pp.1140-1142, 1975.

33. Li, M. K. and H. S. Fogler, "Acoustic Emulsification Part 2. Breakup of the Large Primary Oil Droplets in a Water Medium", *Journal of Fluid Mechanics*, Vol.88, pp.513-528, 1978.

34. Bromley, L. A., "Heat Transfer in Stable Film Boiling," *Chem. Eng. Prog.*, Vol. 46, pp. 221, 1950.

35. Moriyama, K., N. Yamano, Y. Maruyama, T. Kudo and J. Sugimoto, *ALPHA Visual Data Collection Stx005-025: Melt Drop Steam Explosion Experiments*, Jaeri-Data/Code 99-017, March 1999.

36. Bates, J. L., C. E. McNeilly, and J. J. Rasmussen, "Properties of Molten Ceramics", *Ceramics in Severe Environments*, Vol. 5, Material Science Research, Plenum Press, New York, pp. 11-25, 1971.

37. Blomquist, R. A., J. K. Fink and L. Leibowitz, "Viscosity of Molten Alumina", *American Ceramic Society Bulletin*, 57 (5), 1978.

38. Fletcher, D. F., "An Improved Mathematical Model of Melt/Water detonations-1. Model Formulation and Example Results", *International Journal of Heat and Mass Transfer*, Vol. 34, No. 10, pp. 2435-2448, 1991

39. Fletcher, D. F., "An Improved Mathematical Model of Melt/Water detonations-ll. A Study of Escalation", *International Journal of Heat and Mass Transfer*, Vol. 34, No. 10, pp. 2449-2459, 1991.

40. Fletcher, D. F. and A. Thyagaraja, "A Mathematical Model of Melt/Water Detonations", *Appl. Math. Modeling*, Vol. 13, pp. 339-347, 1989.

41. Fletcher, D. F., *Modeling Transient Energy Release From Molten Fuel Coolant Interaction Debris*, AEE Winfrith Report, AEEW-M2125, 1984.

42. Derewnnicki, K. P., "Experimental Studies of Heat Transfer and Vapor Formation in Fast Transient Boiling", *International Journal of Heat and Mess Transfer*, Vol. 28, pp. 2085-2092, 1985.

43. Furuya, M., I. Kinoshita and Y. Nishi, "Explosive Fragmentation of an Impinging Droplet Interacted with a Molten Alloy Pool", *Proceedings of the International Seminar on Vapour Explosions and Explosive Eruptions*, Sendai-Japan, pp. 75-81, 1997.

44. Yamano, N., Y. Maruyama, T. Kudo, A. Hidaka and J. Sugimoto, "Phenomenological Studies on Melt-Coolant interactions in the ALPHA Program", *Nuclear Engineering and Design*, Vol.155, pp.369-389, 1995.

REFERENCES NOT CITED

Abolfadl, M. A. and T. G. Theofanous, "An Assesment of Steam Explosion Induced Containment Failure Part II: Premixing Limits ", *Nuclear Science and Engineering*, Vol. 97, pp. 282-295, 1987.

Angelini, S., E. Takara, W. W. Yuen and T. G. Theofanous, "Multiphase Transients in the Premixing of Steam Explosions", *Nuclear Engineering and Design*, Vol. 146, pp. 83-95, 1994.

Angelini, S., W. W. Yuen and T. G. Theofanous, "Premixing Related Behavior of Steam Explosions", *Nuclear Engineering and Design*, Vol. 155, pp. 115-157, 1995.

Board, S. J., C. L. Farmer and D. H. Poole, "Fragmentation in Thermal Explosions", *International Journal of Heat and Mass Transfer*, Vol. 17, pp. 331-339, 1974.

Buchanan, D. J., "A Model for Fuel Coolant Interactions", *Journal of Phys. D: Applied Physics, Vol. 7, pp. 1441-1457, 1974.*

Cho, D. H., D. R. Armstrong and R. P. Anderson, "Combined Vapor and Chemical Explosions of Metal and Water", *Nuclear Engineering and Design*, Vol. 155, pp. 405-412, 1995.

Chu, C. C. and M. L. Corradini, "One Dimensional Transient Fluid Model for Fuel /Coolant Interaction Analysis", *Nuclear Science and Engineering*, Vol. 101, pp. 48-71, 1989.

Condiff, D. W., "Contributions Concerning Quasy-Steady Propagation of Thermal Detonations Through Dispersions of Hot Liquid Fuel in Cooler Volatile Liquid Coolants", *International Journal of Heat and Mass Transfer*, Vol. 25, pp. 87-98, 1982.

Corradini, M. L., "Analysis and Modeling of Large-Scale Steam Explosion Experiments", *Nuclear Science and Engineering*, Vol. 82, pp. 429-447, 1982.

Dowling, M. F., B. M. Ip and S. L. Abdel-Khalik, "Supresion of Vapor Explosions by Dilute Aqueous Polymer Solutions", *Nuclear Science and Engineering*, Vol. 113, pp. 300-313, 1993.

Drumheller, D. S., " The Initiation of Melt Fragmentation in Fuel Coolant Interactions", *Nuclear Science and Engineering*, Vol. 72, pp. 347-356, 1979.

Epstein, E. and H. K. Fauske, "A Crystallization Theory of Underwater Aluminum Ignition", *Nuclear Engineering and Design*, Vol. 146, pp. 147-164, 1994.

Epstein, M., "Thermal Fragmentation-a Gas Release phenomenon", *Nuclear Science and Engineering*, Vol. 55, pp. 462-467, 1974.

Fletcher, D. F., "Vapor Explosions: Multiphase Detonations or Deflagrations?", *Shock Waves*, Vol. 3, pp. 181-192, 1994.

Henry, R. E., "Externaly Triggered Steam Explosion Experiments: Amplification or Propagation?", *Nuclear Engineering and Design*, Vol. 155, pp. 37-44, 1995.

Han, S. H. and S. G. Bankoff, "An Unsteady one-dimensional two fluid model for Fuel Coolant Mixing", *Nuclear Engineering and Design*, Vol. 95, pp. 285-295, 1986.

Henry, R. E. and H. K. Fauske, "Nucleation Processes in Large Scale Vapor Explosions", *ASME Journal of Heat Transfer*, Vol. 101, pp. 280-287, 1979.

Hohmann, H., D. Magallon, H. Schins and A. Yerkes, "FCI Experiments in the Aluminum Oxide/ Water System", *Nuclear Engineering and Design*, Vol. 155, pp. 391-403, 1995.

Inoue, A., and S. G. Bankoff, "Destabilization of Film Boiling Due to Arrival of a Pressure Shock. Part I: Experimental", *ASME Jounal of Heat Transfer*, Vol. 103, pp. 459-464, 1981.

Inoue, A., A. Ganguli and S. G. Bankoff, "Destabilization of Film Boiling Due to Arrival of a Pressure Shock. Part II: Analytical", *ASME Jounal of Heat Transfer*, Vol. 103, pp. 465-471, 1981.

Medhekar, S., M. Abolfadl and T. G. Theofanous, "Triggering and Propagation of Steam Explosions", *Nuclear Engineering and Design*, Vol. 126, pp. 41-46, 1991

Nelson, L. S., "Steam Explosions of Single Drops of Pure and Alloyed Aluminum", *Nuclear Engineering and Design*, Vol. 155, pp. 413-425, 1994.

Patel, P. D. and T. G. Theofanous, "Hydrodynamic Fragmentation of Drops", *Journal of Fluid Mechanics*, Vol. 103, pp. 207-223, 1981.

Pilch, M., and C. A. Erdman, "Use of Breakup Time Data and Velocity History Data to Predict the Maximum Size of Stable Fragments for Acceleration-Induced Breakup of a Liquid Drop", *International Journal of Multiphase Flow*, Vol. 13, pp. 741-757, 1987.

Schins, H., "Characterization of Shock Triggers Used in Thermal Detonation Experiments", *Nuclear Engineering and Design*, Vol. 94, pp. 93-98, 1986.

Theofanous, T. G., X. Chen, P. D. Piazza, M. Exptein and H. K. Fauske, "Ignition of Aluminum Droplets Behind Shock Waves in Water", *Phys. Fluids*, Vol. 6 pp. 3513-3515, 1994.

Yang, J. W. and S. G. Bankoff, "Solidification Effects on the Fragmentation of Molten Metal Drops Behind a Pressure Shock Wave", *ASME Journal of Heat Transfer*, Vol. 109, pp. 226-231, 1987.